ANALYSIS OF THE REACTIVITY COEFFICIENTS AND THE STABILITY OF A BWR LOADED WITH MOX FUEL

Ch. Demazière
Department of Reactor Physics
Chalmers University of Technology
SE - 412 96 Göteborg
Sweden
demaz@nephy.chalmers.se

ABSTRACT

In the past few years, the use of MOX fuel in commercial nuclear power stations has been considered in the western countries. France has already developed an extensive reprocessing program based on the use of uranium-plutonium mixed oxide fuel in PWRs. Whereas most of the electricity in France is provided by PWRs, the BWR type is predominantly used in USA, Japan, Germany, Sweden, and some of these countries plan to load MOX bundles in BWRs. The aim of this study is to model the impact of a core-loading pattern containing MOX bundles upon the main characteristics of a BWR (reactivity coefficients, stability).

For this purpose, the Studsvik Scandpower code package (CASMO-4/TABLES-3/SIMULATE-3[1-3]) is used since it has been shown that these codes are able to accurately represent and model MOX bundles. This study is thus devoted to the modelling of BWR cores (of the General Electric BWR/6 type) loaded partially (approximately 2/3 of UOX bundles and 1/3 of MOX bundles) or totally with MOX bundles. The plutonium quality used is the Pu type 2016 (mostly Pu-239, 56%, and Pu-240, 26%), but a variation of the plutonium isotopic vector is also investigated, in case of a partial MOX loading. One notices that the reactivity coefficients do not show significant changes in comparison with a full UOX loading. Nevertheless, two main problems arise: the shutdown margin at BOC is lower than 1% and the stability to in-phase oscillations is decreased.

1. INTRODUCTION

In the past few years, the use of MOX fuel in commercial nuclear power stations has been

considered in some western countries. Among them, France is probably the most experienced one, since it has extensively developed a reprocessing program based on the use of uranium-plutonium mixed oxide fuel in PWRs (Pressurized Water Reactors).

Whereas most of the electricity in France is provided by 54 nuclear reactors, which are of the PWR type and one fast breeder reactor (Phenix in Marcoule), the BWR type is predominantly used in USA, Japan, Germany and in Sweden. Except for the United States, the three other countries plan to load MOX bundles in BWRs. This MOX program is still marginal in Germany and in Sweden. But Japan wants to develop an important MOX program in BWRs (a 100 % MOX ABWR - Advanced Boiling Water Reactor - has been announced for the next decade).

Consequently, CEA (the French Atomic Energy Commission) has to study the ability of BWRs to be loaded with MOX fuel: firstly because it is one of its research duties, and secondly because some of the French nuclear power plants have to be renewed by 2010-2020 and the BWR type could be a promising challenger. Then the following question arises: how does a BWR behave with MOX fuel? This is precisely the goal of this “preliminary” study.

More specifically, one has to define a MOX (and also a UOX) bundle which fulfils a few requirements, such as the cycle length, and allows avoiding any power peak. With these bundles, a loading pattern strategy has to be found; a core equilibrium model must also be developed since it is the only way of comparing cores with different characteristics. Finally, the safety parameters, the reactivity coefficients and the stability have to be characterized; both a partial MOX loading and a full MOX loading have to be investigated, and for the partial one a sensitivity study to the plutonium quality has to be conducted.

2. DETERMINATION OF THE UOX AND THE MOX BUNDLES

In order to study the ability of BWR cores to be loaded with MOX bundles and to develop a core equilibrium model, several types of bundles are necessary. First of all, one needs fresh UOX fuel, which will constitute the first loading (cycle 1). One also needs fresh UOX fuel that will be used for a full UOX loading and that will be loaded according to the same strategy from cycle to cycle until the equilibrium core is reached. Since the main aim of this project is to compare the MOX cores to the UOX cores, it was decided to use typical UOX bundles for these aforementioned ones. They are of the General Electric 8x8 type and are based on reference 4.

From this full UOX equilibrium (after 15 cycles), a MOX equilibrium (after 15 cycles also) must be reached, either in a partial MOX loading or a full MOX loading. This requires defining both a UOX and a MOX bundle, since the properties of one bundle depend on its environment. Nevertheless, the same MOX bundle was used for both the partial and the full MOX loading, since the bundle optimization process is rather cumbersome.

2.1 METHODOLOGY

As the mechanical design of the different bundles is assumed to correspond to the General Electric BWR 8x8 type, it only remains to determine the enrichment of the different pins (either in U-235, or in Pu) and the location of the gadolinium pins. Even for this simple task, optimizing the lattices requires four main steps, as described below. All the calculations have been performed at 40 % of void, since it is approximately the core-average void content.

- *<u>Step 1:</u> predertermination of the average enrichment (either in U-235, or in Pu) in order to achieve the desired cycle length*

For the MOx bundle, it is necessary to define the quality of plutonium, which is used in this study. The plutonium isotopic vector is referenced as Pu type 2016, which corresponds to the expected plutonium quality that will be available in France in 2016, due to the reprocessing activities. This quality is defined in Table I below.

Table I: Nominal Plutonium Isotopic Vector

Pu isotope	mass fraction (%)
Pu-238	2,7
Pu-239	56,0
Pu-240	25,9
Pu-241	8,1
Pu-242	7,3

One also needs to know the cycle characteristics, assuming that they can be applied to each cycle in the equilibrium model, as described in Table II below.

Table II: Cycle Characteristics for a General Electric BWR/6

Cycle length	369 days (≈ 12,3 months)
Capacity factor	85 %
Cycle length at full power	314 EFPD (Effective Full Power Days)
Power density	50 kW/l
Core rated thermal power	3380 MWth
Core rated flow	$47{,}25.10^6$ kg/hr
Heated fraction of flow	85 %
Number of assemblies	764

Table II: Cycle Characteristics for a General Electric BWR/6

Assembly nominal active fuel height	381 cm (cold)
Fraction of discharged bundles	≈ 1/4
UOX bundles fuel density EOC core-average burnup	 10,3 g/cm^3 19,061 GWd/tHM
MOX bundles fuel density EOC core-average burnup	 9,78 g/cm^3 20,075 GWd/tHM

The fuel density has been reduced for the MOX bundle in order to approach the moderator to fuel ratio optimum (this optimum is greater for MOX fuel since the multiplication factor is higher due to Pu-239). This fuel density still allows keeping an undermoderated lattice at EOL (End Of Life) as can be seen in Fig. 1 below.

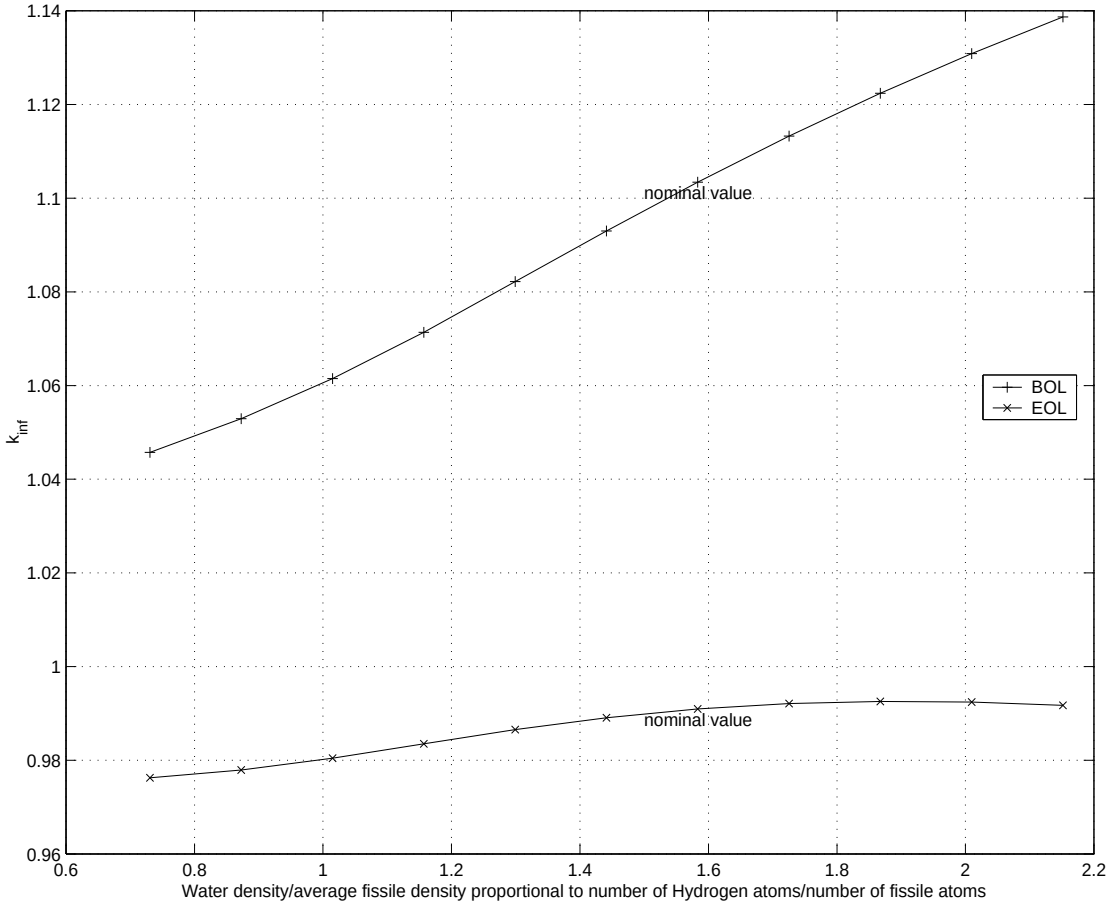

Fig. 1 Variation of Lattice Multiplication Factor for the MOX Bundle Versus Moderator/Fuel Ratio (Void Change Only)

This is an important feature since the shape of the multiplication factor curve also affects void coefficients (and temperature coefficients) of reactivity. The greater the slope of the curve, the more negative the coolant density reactivity coefficient is.

Since the effective multiplication factor should be equal to unity for the core-average burnup given in Table II, one can estimate the corresponding infinite multiplication factor for a fuel bundle:

$$k_\infty = 1 + M^2 B_g^2 \times 2,5 \tag{1}$$

where the geometrical buckling can be approximated by:

$$B_g^2 = \left(\frac{j_0}{R_c}\right)^2 + \left(\frac{\pi}{H_c}\right)^2 \tag{2}$$

R_c and H_c are the core radius and core height respectively (extrapolation length neglected). j_0 is the first root of the J_0 Bessel function. The factor 2,5 allows representing the actual leakage in the bundle from the geometrical buckling (value commonly used).

A depletion calculation with a uniform lattice is then necessary to calculate the reactivity at this burnup. CASMO-4 can be used for this purpose. This means that the methodology is a trial-error strategy: for a given average enrichment, the infinite multiplication factor is calculated for the core-average burnup (given in Table II), the corresponding effective multiplication factor is deduced, and according to the deviation from unity, the average enrichment is consequently increased or decreased. The migration area M^2 is calculated by CASMO-4 and can be considered almost constant during the fuel depletion. This procedure is repeated until an enrichment is found with which Eq. (1) is satisfied.

- <u>*Step 2:*</u> *Optimization process in order to avoid any power peak inside the bundle and to keep the expected cycle length*

Let us assume that one modifies the lattice that was obtained in step 1 in order to flatten the power distribution inside the bundle. This new lattice will probably not give the requested infinite multiplication factor at the EOC core-average burnup (EOCCAB). If one assumes that:

$$k_{\infty,\,requested}^{BOL} - k_\infty^{BOL} \approx k_{\infty,\,requested}^{EOCCAB} - k_\infty^{EOCCAB} \tag{3}$$

the first-order perturbation theory (in one-group approximation) can be used to calculate the initial enrichment that allows fulfilling the reactivity requirement at the EOC core-average burnup:

$$\delta\rho = -\delta\left(\frac{1}{k_\infty}\right) = \frac{\delta k_\infty}{k_\infty^2} = \frac{\frac{1}{k_\infty}\delta(\nu\Sigma_f) - \delta\Sigma_a}{\nu\Sigma_f} \tag{4}$$

The adjustment of the power peaks is carried out by optimizing the pin power distribution:

$$P_{pin} = \sum_{nuclides\ X \in U, Pu} N_X \sigma_{f,X} \kappa_X \phi \qquad (5)$$

Thus the relative power fraction (RPF) of a pin in comparison to the total bundle power (assumed to be constant in the CASMO-4 modelling) is proportional to this quantity. Assuming that the flux in a pin can be considered, in a first approximation, as a constant if one modifies the enrichment of the pin, one can relate the change in the enrichment needed to obtain a flat power distribution.

Consequently, from the characteristics of a lattice, one can estimate a "better" lattice that allows flattening the power distribution, while keeping the expected cycle length. Then CASMO-4 is used to deplete this new lattice. And depending on the results obtained via CASMO-4, one can re-apply this optimization process.

- *<u>Step 3:</u> Determination of the location of the Gd pins*

The determination of the location of the Gd pins is the result of a compromise between the following criteria:

- one must avoid any mismatch between the Gd depletion and the fuel depletion: if the Gd depletion is too rapid, the excess reactivity at BOL remains; if the Gd depletion is too slow, the negative reactivity due to Gd is still significant at the EOC core-average burnup and implies a shorter cycle length;
- the Gd can also be used to reduce the power peaks;
- because of the strong capture of thermal neutrons due to Gd, the efficiency of the control rods has to be checked.

Consequently, one must locate the Gd in pins where the flux is not too high in order to avoid any too rapid consumption. On the other hand, one must also keep in mind that the flux in the Gd pins must not be too low, otherwise the Gd will not be depleted at the EOC core-average burnup, which results in a decrease of reactivity and then a shorter cycle length.

As a matter of fact, one must find a compromise between these two behaviours. Also we recall that if the Gd is put into pins with too low flux, the effects of Gd are not even perceptible. Secondly, the Gd could also allow reducing the relative power fraction in the pins where the power is too high. But most of the time, these regions coincide with high thermal flux regions, that is to say regions in which the use of Gd is not recommended because of the mismatch effect. Finally, one must keep in mind that, because of the strong capture of thermal neutrons in Gd, the efficiency of the control rods has to be checked (only at BOL since the Gd absorption decreases with the fuel depletion). This is particularly important when the Gd pins are located near the control rods, i.e. along the wide water gap.

One must also say that, for the Gd pins, one has to use UOX pins instead of MOX pins. As one of the main goals of the MOX bundle is to maximize the Pu utilization, increasing the number of UOX pins is not a judicious choice. This is why the Gd pins must be as effective as possible.

There is no other possibility than testing the different locations for the Gd pins according to the

following methodology:

- for each region separately, the U-235 content is set to 3,5 % and the Gd content is set to 4,0 % (maximum allowable Gd content for an annual cycle, see reference 4);
- the following points are then checked:
  - is there any depletion mismatch between the Gd and the fuel?
  - is the Gd effect perceptible?
  - is the Gd completely depleted before the EOC core-average burnup?
  - what is the power distribution?
  - is the final k_∞ strongly modified?
  - what is the control rod worth?

Then one can find out the most suitable location for the Gd pins. This means also that a re-optimization process is essential.

- *Step 4: Re-optimization process*

Due to the introduction of the Gd pins, it is no longer granted that the effective multiplication factor is close to unity and that the power peaks are avoided. But because of the presence of pins with different properties inside the bundle, there are several ways of optimizing the assembly. The following one has been used for this study.

First, one wants to keep the maximum allowable Gd content in order to reduce the initial reactivity excess as much as possible. Second, the reactivity adjustment (k_{eff} close to unity at the EOC core-average burnup) is realized:

- first by modifying the U-235 enrichment in the Gd pins (it allows avoiding too many modifications in the other pins);
- if the maximum allowable U-235 content in the Gd pins is reached (3,5 % as described beforehand), one modifies the average U/Pu enrichment of the other pins.

If the effective multiplication factor at BOL is lower than unity (but still larger than unity at the EOC core-average burnup), then the Gd content is reduced. We recall that there is no reactivity modification at the EOC core-average burnup due to any Gd change since it has been checked that the Gd is fully depleted before the EOC core-average burnup.

Finally, as the power distribution is significantly modified by the Gd, it must be flattened once more, but only the pins without Gd are concerned by this stage (the UOx pins that contain Gd have a relative power fraction which is significantly lower than unity). Thus a new U/Pu enrichment distribution must be calculated and normalized to the average U/Pu enrichment (which is necessary since the final k_{eff} will be modified).

2.2 LATTICES

This methodology has been applied to BWR General Electric 8x8 bundles. Each bundle has an active height of 381 cm. But at the bottom and the top of each bundle, one uses a blanket of natural uranium. Its function is not only to reflect the neutrons (and consequently to reduce the axial neutron leakage), but also to produce Pu fissile isotopes at the top of the core by conversion from U-238 at high void fraction. Without this blanket, the stretch-out (i.e. operating the reactor at

full power, all rods out, by increasing the core flow) and the succeeding coast-down (i.e. operating the reactor at full core flow, all rods out, but with a decreasing power) would be less effective, that is to say the cycle length would be shorter. Nevertheless, the top of the main segment contributes also to this conversion to a certain extent.

The optimized UOX and MOX segments are presented hereafter in Tables III and IV.

N.B.: A typical UOX BWR 8x8 bundle (from reference 4) was also used in this study as a reference bundle for the full UOX core loading. Its properties are not described in this paper.

Table III: Lattice of the UOX Segment (Southeast Corner)

1							
2	5						
3	6	7					
4	7	7	7				
4	7	8	W	7			
3	6	7	8	7	7		
2	5	6	7	7	6	5	
1	2	3	4	4	3	2	1

Cell	Enrichment
1	1,75 % (U-235/U)
2	2,12 % (U-235/U)
3	2,43 %(U-235/U)
4	2,62 %(U-235/U)
5	2,72 % (U-235/U)
6	3,28 % (U-235/U)
7	3,50 % (U-235/U)
8	3,50 % (U-235/U) - 4,0 % (Gd_2O_3/oxide)

Table IV: Lattice of the MOX Segment (Southeast Corner)

1							
2	5						
3	7	11					
4	8	11	6				
4	8	9	W	6			
3	7	10	9	11	11		
2	5	7	8	8	7	5	
1	2	3	4	4	3	2	1

Cell	Enrichment
1	1,56 % (Pu/U+Pu)
2	2,35 % (Pu/U+Pu)
3	3,03 % (Pu/U+Pu)
4	3,43 % (Pu/U+Pu)
5	2,97 % (U-235/U) - 4,0 % (Gd_2O_3/oxide)
6	9,52 % (Pu/U+Pu)
7	5,74 % (Pu/U+Pu)
8	6,87 % (Pu/U+Pu)
9	9,56 % (Pu/U+Pu)
10	8,58 % (Pu/U+Pu)
11	10,30 % (Pu/U+Pu)

For the top and bottom segments, all the fuel pins contain 0,71 % of U-235 (in mass).

2.3 PROPERTIES

The infinite multiplication factor of the UOX and the MOX segments (CASMO-4 calculations)

are presented in Figs. 2 and 3 respectively.

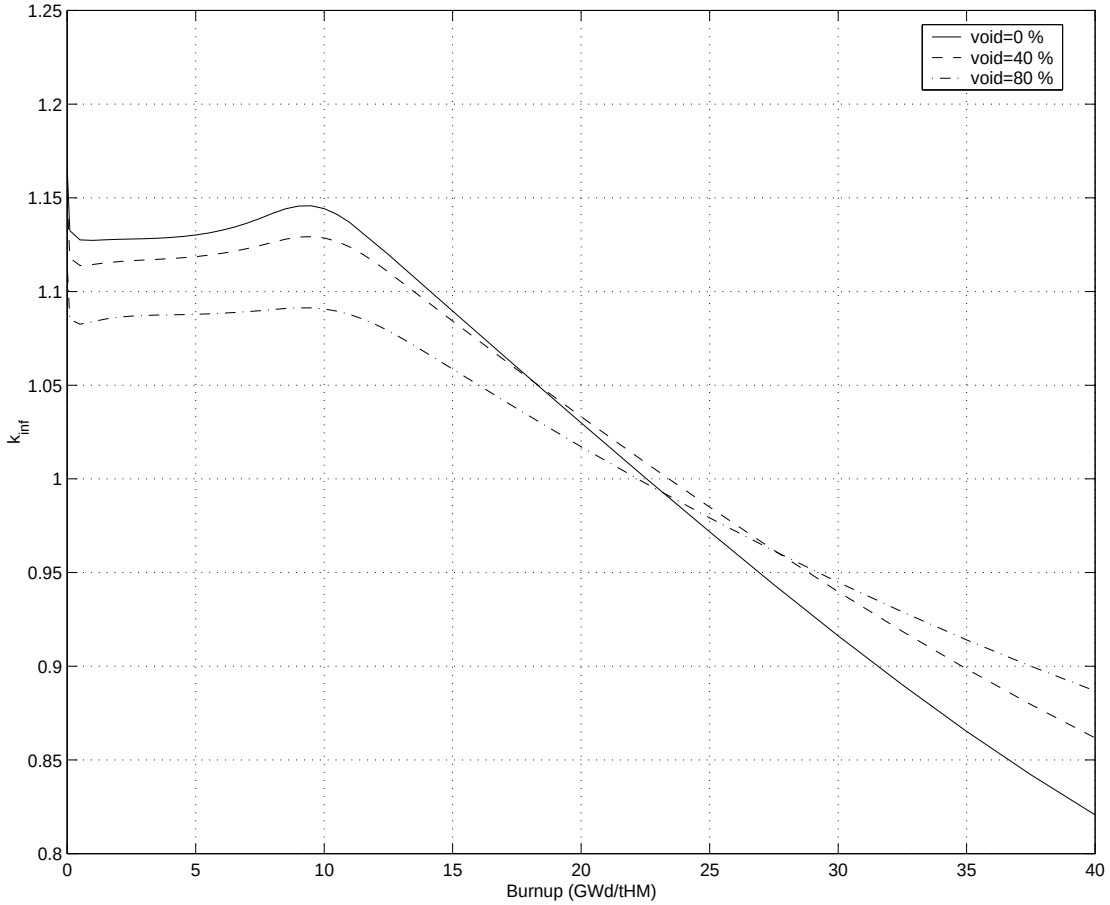

Fig. 2 Infinite Multiplication Factor of the UOX Segment (at Hot Conditions, Without Control Rod)

Because of the larger absorption cross-section of plutonium fuel, power discontinuities can occur at boundaries between UOX and MOX bundles. It is thus necessary to check the properties of the UOX and MOX segments in a checkerboard pattern, via the use of CASMO-4 (see Table V, Figs. 4, 5, and 6).

Table V: Comparison Between the UOX and the MOX Segments in a Checkerboard Pattern

	At 0 GWd/tHM		At 40 GWd/tHM	
	UOX	MOX	UOX	MOX
Burnup (GWd/tHM)	0,000	0,000	38,302	41,788
$\nu\Sigma_f/\Sigma_a$	1,13827	1,11642	0,87403	0,93249
2-group k_∞	1,14816	1,10338	0,87952	0,92650

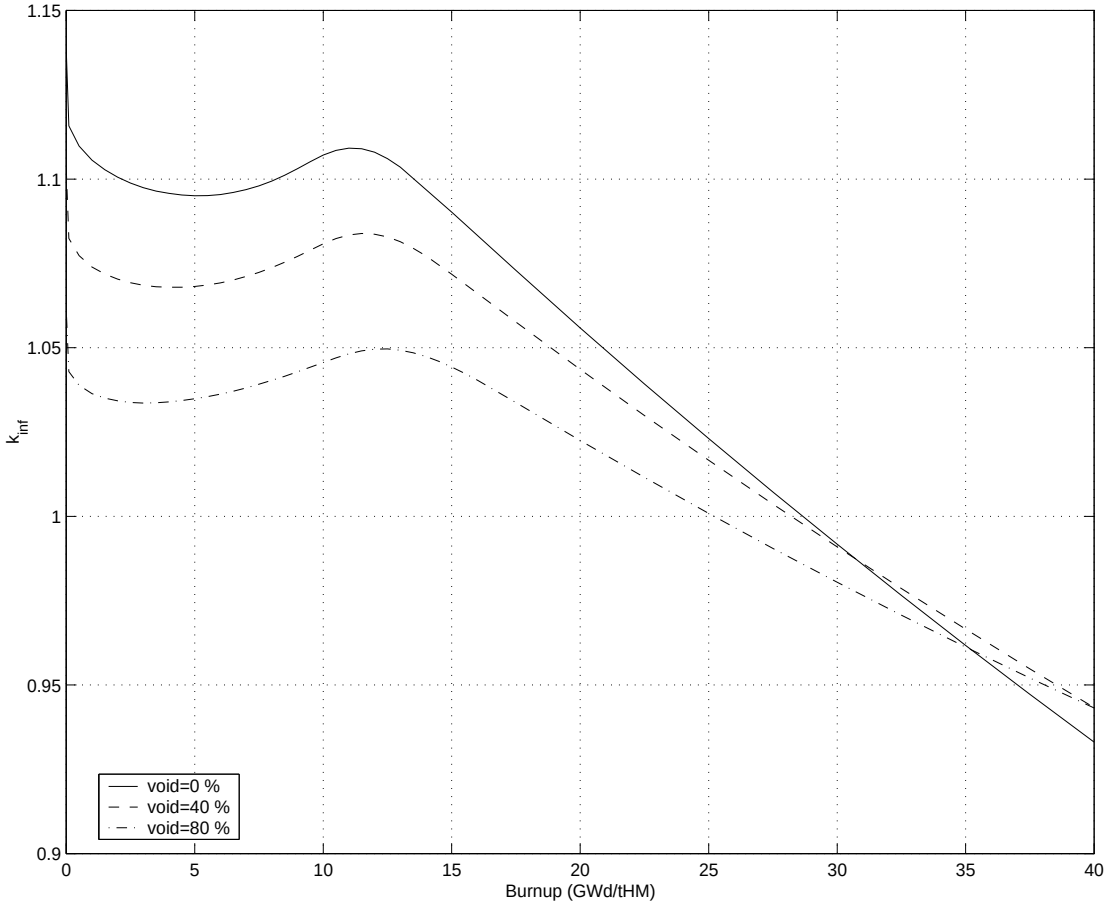

Fig. 3 Infinite Multiplication Factor of the MOX Segment (at Hot Conditions, Without Control Rod)

Table V: Comparison Between the UOX and the MOX Segments in a Checkerboard Pattern

	At 0 GWd/tHM		At 40 GWd/tHM	
	UOX	MOX	UOX	MOX
2-group M^2 (cm^2)	86,11	83,77	87,69	87,84
Fission fraction	1,023	0,977	0,941	1,059
Absorption fraction	0,943	1,057	0,959	1,041
Nu*fission fraction	0,952	1,048	0,927	1,074
Power fraction	1,009	0,991	0,938	1,062

One notices that the UOX bundle contributes to most of the energy release at BOL, whereas the contribution of the MOX bundle becomes more significant during the depletion and even larger than the UOX one. This is mostly due to the higher macroscopic absorption cross-section in the MOX segment at BOL, in comparison with the UOX segment. Consequently, the depletion rate is

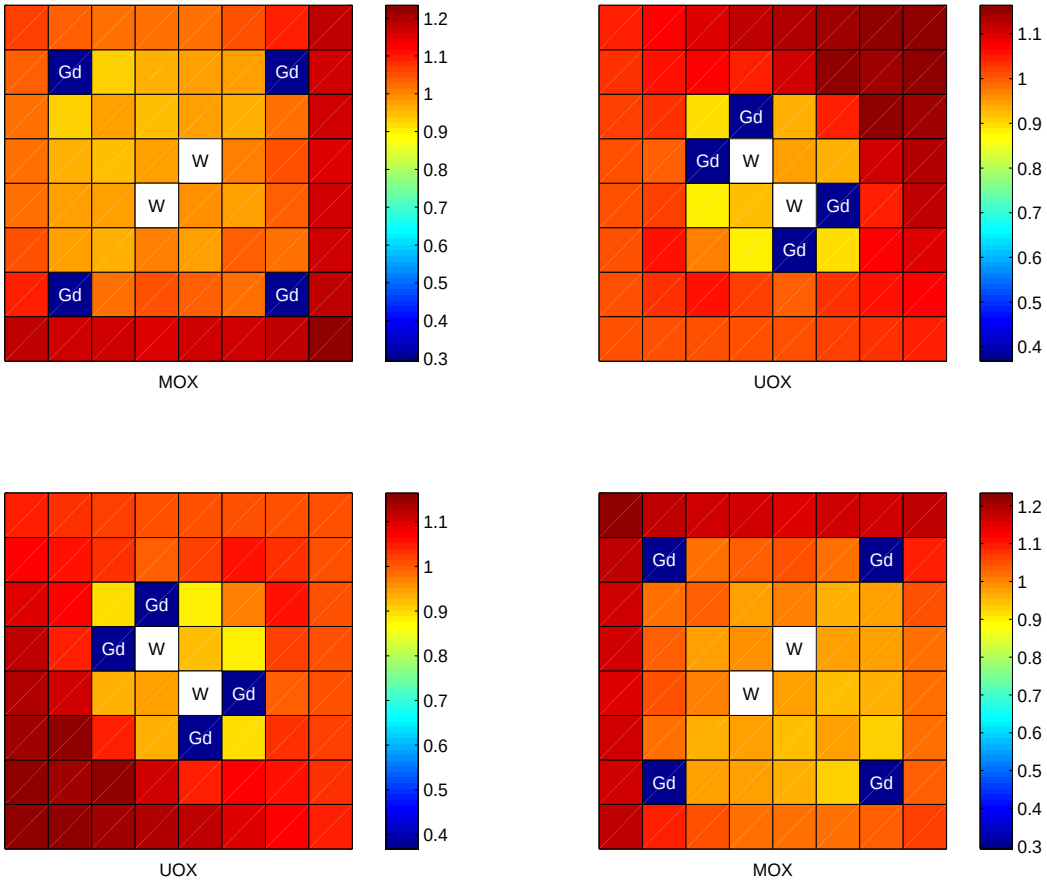

Fig. 4 Power Distribution in the UOX and MOX Segments in a Checkerboard Pattern at BOL (40 % of Void)

higher in the MOX segment, this is why the corresponding burnup is larger at EOL. Since the infinite multiplication factor for the MOX segment at hot conditions without control rod is greater than the one for the UOX segment at high burnup, the relative importance of the MOX bundle becomes more significant during the depletion. As expected also, the flux is harder in the MOx bundle because the thermal absorption is much larger (the corresponding macroscopic absorption cross-section is greater). Finally, the power distribution is relatively good during the depletion. The power peak for the MOX bundle is moving from the periphery at BOL towards the centre of the assembly at EOL, since the depletion rate is larger along the (wide) water gaps. For the UOX bundle, the power peak located along the water gaps at BOL totally vanishes during the fuel depletion.

3. SIMULATION OF THE LOADING OF THE BUNDLES

In order to be able to compare the different cores (core with a full UOX loading, core with a mixed UOX/MOX loading, core with a full MOX loading), one has to define a common “strategy” for them, i.e. one has to apply the same rules to reload the cores. Furthermore, only the cores that

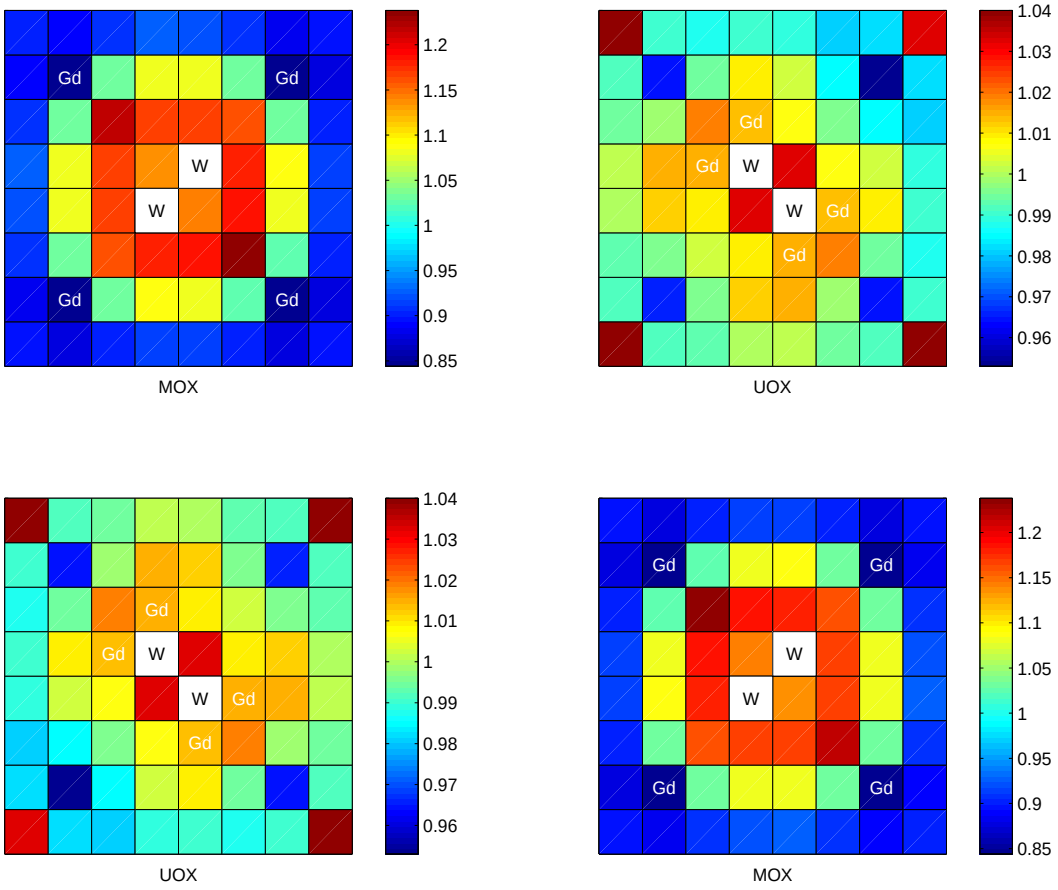

Fig. 5 Power Distribution in the UOX and MOX Segments in a Checkerboard Pattern at EOL (40 % of Void)

have reached equilibrium, i.e. cores that have the same properties from cycle to cycle if one applies the same reloading pattern, can be used for these comparisons. An equilibrium core is a hypothetical model, since the characteristics of the fresh bundles (and also the loading pattern strategy) actually vary from cycle to cycle. But it is the only way of comparing the different cores; otherwise these comparisons would not only depend on the core properties and the interpretation of the differences would become difficult.

3.1 LOADING PATTERN

Determining the “best” loading pattern was clearly out of the scope of this study. This is why the Control Cell Core (CCC) strategy was used for its simplicity and its performances. In the CCC, the control of the reactor is limited to a fixed group of control rods (rods in the A2 control cells) and low reactivity fuel assemblies surround the control rods (see reference 5). The CCC strategy has several advantages such as:

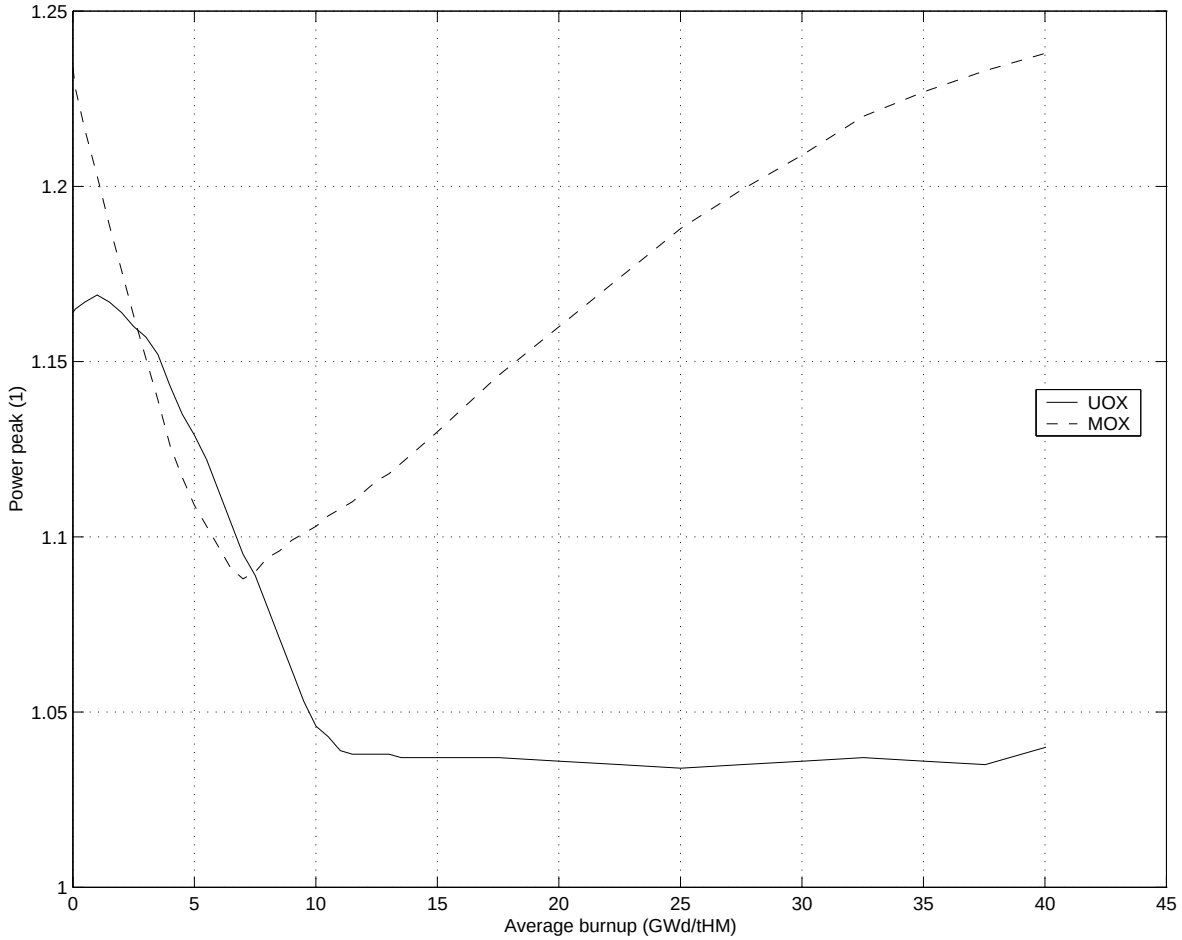

Fig. 6 Power Peaks in the UOX and MOX Segments in a Checkerboard Pattern (40 % of Void)

- reducing the axial power peaking at the tips of the control blades: when the control rod is lowered out of the core, the low reactivity fuel assemblies minimize the effect of suddenly increasing the neutron flux to that portion of the fuel assembly previously shadowed by the control rod;
- minimizing increases in the Linear Heat Generation Rate (LHGR);
- simplifying BWR operation;
- improving BWR capacity factors.

Then the CCC loading strategy can be divided in five main steps (see reference 4):

- discharge of the high burnup assemblies and loading of the fresh fuel;
- loading of the lowest reactivity fuel (highest burnup batches) in the periphery locations (radial blanket);
- loading of the next least reactive fuel in the A2 control cells (from the centre of the core to the core periphery, in order to flatten the power distribution);
- loading of the next least reactive fuel in the cells containing at least one fresh fuel in order to avoid any shutdown margin (SDM) problem (from the centre of the core to the periphery);
- loading of the remaining fuel bundles in the remaining locations (from the periphery of the core to the centre, in order to flatten the burnup distribution).

For the mixed loading, approximately one third of the core is constituted by MOX bundles (280 MOX assemblies, and 484 UOX assemblies for the whole core).

3.2 EQUILIBRIUM CYCLE MODELLING

Once the loading pattern has been chosen, it remains to determine how the fuel will be depleted. This may seem to be a trivial task. Nevertheless, since a BWR is always operated with the control rods inserted (except during the stretch-out and the coast-down), the fuel depletion depends very much on the control rod position. Furthermore, there are several kinds of control rods, so that determining the control rod pattern becomes a cumbersome process. Finally, the core flow is also modified to reach criticality (the differential control rod worth is too large in a BWR to allow such a precise adjustment). Simply speaking, the control rods are first adjusted such that most of the hot excess reactivity in the reactor is counteracted by the negative reactivity of the control rods. The core flow is then adjusted to maintain criticality (by the negative void coefficient). As the hot excess reactivity changes throughout the cycle, the control rod pattern is adjusted to compensate the hot excess.

One of the main advantages of the CCC strategy is that only the rods in the A2 control cells are used. But these rods do not belong to a unique bank, as it could be for a PWR for instance, i.e. the insertion is different from rod to rod. Consequently, determining the control rod positions is a cumbersome trial-error optimization process, which was clearly out of the scope of this preliminary study. Furthermore, since this control rod pattern would be different between the full UOX loading, the mixed UOX/MOX loading, and the full MOX loading, comparing these various loadings becomes difficult. This is why a different approach was used in this study. The depletion was carried out in accordance with the Haling principle (see reference 5), which is a hypothetical depletion, but which could be applied to any loading. The Haling principle states that “The minimum peaking factor for a given fuel loading arrangement is achieved by operating the reactor so that the power shape (power distribution) does not change appreciably during the operating cycle”.

Based on this Haling principle, an equilibrium model was developed for each loading. An equilibrium cycle consists of establishing a loading pattern using a fresh batch of fuel (fixed number of assemblies at a fixed enrichment) and then depleting and shuffling using the same fuel design and loading pattern for multiple cycles. Equilibrium is reached when exposure and power distributions converge to one solution, which does not change in succeeding cycles. The only constraint that was used in this model was to reach a target effective multiplication factor of 1.00000 ($\pm$ 100 pcm) at EOC. This was realized by modifying the reload batch size (approximately one fourth of the core) and by readjusting the loading pattern accordingly. Optimizing the power distribution and readjusting the enrichment of the bundles were clearly out of the scope of this study.

3.3 PERFORMANCES OF THE EQUILIBRIUM CORES

Table VI below summarizes the results that can be expected with the previous loading patterns. Nevertheless, please keep in mind that the depletion has been carried out without any control rod inserted in the core and that the Haling principle has been applied. Consequently, this equilibrium modelling corresponds to hypothetical cores.

Table VI: Characteristics of the Equilibrium Cores at EOC

Core	Discharge burnup (GWd/tHM)			Batch-average[a] 2D relative power fraction	Batch-average[a] 2D burnup (GWd/tHM)
	Minimum	Average	Maximum		
Full UOX	24,52	26,10	28,28	1,158 1,032 1,057 0,398	8,86 16,76 24,84 26,43
UOX (2/3)	24,18	26,18	29,91	1,185 0,971 1,064 0,541	8,91 16,21 24,18 27,30
MOX (1/3)	29,26	32,16	35,63	1,148 1,147 0,981 0,788 0,495	9,06 18,13 26,19 31,43 32,10
Full MOX	26,22	29,32	33,19	1,160 1,002 1,048 0,744	8,87 16,54 24,55 29,81

a. The batch-average data are given first for the once depleted fuel, then for the twice depleted fuel, and so on.

The transition cycles required to reach the equilibrium model are less numerous for the full UOX loading (approximately 5 or 6 cycles) than for the mixed or the full MOX loading (approximately 8 to 9 cycles). Furthermore, the effective multiplication factor for the full MOX core at EOC still oscillates after these transition cycles.

As explained earlier, the burnup at EOC of the MOX bundles (either for each batch, or the discharged assemblies) is larger than the UOX ones. But one notices also that this “gap” between the MOX fuel and the UOX fuel burnup is much larger in case of a mixed loading. This is due to the fact that a mixed loading pattern introduces power peaks at the interface of the MOX bundles

(with the UOX ones). Thus the absorption rate is improved (greater), and consequently the MOX fuel depletes more rapidly.

4. CORE PROPERTIES

Since one has defined equilibrium cores that are comparable (the only difference between the cores is their MOX loading fraction, and consequently their loading pattern), it is possible to study the influence of the MOX bundles on the core properties. Nevertheless, we recall that the equilibrium cores are hypothetical models, because the equilibrium cannot be reached in practice (applying the same loading from cycle to cycle cannot be done, since the fuel characteristics are always improved).

Thus, several points are worth being studied, and among them the reactivity coefficients, and the stability. For the last one, only a qualitative analysis will be carried out since no transient code is yet available at the Reactor Physics Department, Chalmers University of Technology. But both a qualitative and a quantitative analysis will be executed for the reactivity coefficients.

It was also decided, through these analyses, to model a variation of the Pu isotopic vector in order to see the dependence of the core characteristics with the Pu quality. Variations (in percent) of the Pu-A content Pu^{A}/Pu_{tot} (A=238, 239, 240, 241, or 242) relative to its nominal value were modelled. It means that not only a variation of the Pu-A content is studied, since the concentration of the other Pu isotopes is varying (this is due to the total amount of Pu being kept constant). A variation of ± 50 % relative to the nominal Pu isotopic vector has been modelled.

4.1 ANALYSIS OF THE REACTIVITY COEFFICIENTS

Let us first perform a qualitative analysis of the reactivity coefficients via CASMO-4. This analysis mostly relies on the four-factor formula. This is why one needs CASMO-4 to determine the contribution of each factor to the effective/infinite multiplication factor. This can be still regarded as a qualitative study since one is only interested in the variation of these factors with the fuel temperature, or the void content. The numerical values associated with these changes are completely disregarded.

The four-factor formula can be expressed as:

$$k_{eff} = \varepsilon p f \eta \frac{e^{-\tau B^2}}{1 + L^2 B^2} \tag{6}$$

where:
- ε is the fast fission factor;
- p is the resonance escape probability;

- f is the thermal utilization factor;
- η is the thermal fission factor;
- τ is the Fermi age;
- L is the diffusion length;
- B^2 is the buckling.

After differentiation, one obtains:

$$\frac{1}{k_{eff}}\frac{\partial k_{eff}}{\partial P} = \frac{1}{\varepsilon}\frac{\partial \varepsilon}{\partial P} + \frac{1}{p}\frac{\partial p}{\partial P} + \frac{1}{f}\frac{\partial f}{\partial P} + \frac{1}{\eta}\frac{\partial \eta}{\partial P} - \left(\tau + \frac{L^2}{1+L^2B^2}\right)\frac{\partial B^2}{\partial P} - \frac{L^2}{1+L^2B^2}\frac{\partial L^2}{\partial P} - B^2\frac{\partial \tau}{\partial P} \quad (7)$$

where P is the parameter which is modified (fuel temperature, void fraction, etc.). But one must define precisely the fast fission factor ε since the way of "counting" the neutrons in a modern transport code like CASMO-4 is different from the four-factor formula. The following expressions will be used (please note that all the factors except ε have their usual meaning and definition):

$$k_\infty = (\eta f)_2 \varepsilon p = \frac{\nu\Sigma_{f_1}}{\Sigma_{a_1}+\Sigma_{rem}} + \left(\frac{\nu\Sigma_{f_2}}{\Sigma_{a_2}}\right)\times\left(\frac{\Sigma_{rem}}{\Sigma_{a_1}+\Sigma_{rem}}\right) = (\eta f)_1 \times (1-p) + (\eta f)_2 \times p \quad (8)$$

with:

- $p = \frac{\Sigma_{rem}}{\Sigma_{a_1}+\Sigma_{rem}}$;
- $(\eta f)_1 = \frac{\nu\Sigma_{f_1}}{\Sigma_{a_1}}$;
- $(\eta f)_2 = \frac{\nu\Sigma_{f_2}}{\Sigma_{a_2}}$;
- $\varepsilon = \frac{(\eta f)_1 \times (1-p) + (\eta f)_2 \times p}{(\eta f)_2 \times p}$.

It is now possible to analyse the different reactivity coefficients.

Qualitative analysis of the fuel temperature (Doppler) coefficient

The so-called "Doppler broadening of the resonances" is due to the fact that as the temperature of the fuel rises, the thermal vibration of the fuel nuclei also increases. Consequently the range of neutron energies which corresponds to the increased thermal vibration of the fuel nuclei also increases, and the resonance peaks in the absorption cross-sections of the fuel nuclei are

broadened. Overall, the increase in temperature and broadening of the resonances leads to increased resonance neutron absorption in the fuel. Please also recall that the Doppler effect does not modify the resonance integral

$$I = \int \sigma_a(u)du \tag{9}$$

but the effective resonance integral

$$I_{eff} = \int \sigma_{a,\,eff}(u)du = \int \sigma_a(u)\varphi(u)du \tag{10}$$

is varying, where $\varphi(u)$ is the microscopic flux at the lethargy u. And the sign of the Doppler coefficient depends on the competition between the capture rate and the fission rate variations.

As can be seen on the following figures (see Figs. 9, 10, and 11), the most important effect induced by a fuel temperature rise is the decrease of the resonance escape probability in the resonance group (and also the variation of η in the resonance group).

As a matter of fact, the resonance escape probability can be approximated by:

$$p \approx \exp\left(-\frac{V_f N_f I_{eff}}{V_m N_m (\xi\sigma_s)_m}\right) \tag{11}$$

if one considers a homogeneous mixture of a single resonant absorber with water (the subscript *f* denotes the fuel, whereas the subscript *m* denotes the moderator). *V*, *N*, ξ, and σ_s represent the volume, the density, the average lethargy gain per collision, and the scattering microscopic cross-section respectively.

After differentiation, one gets:

$$\frac{1}{p}\frac{\partial p}{\partial T} \approx \ln p \times \frac{1}{I_{eff}}\frac{\partial I_{eff}}{\partial T} \tag{12}$$

Since $\frac{\partial I_{eff}}{\partial T} > 0$ and $p \le 1$, $\frac{1}{p}\frac{\partial p}{\partial T} < 0$.

N.B.1: The increased resonance absorption gives rise to a very small positive contribution due to decreased leakage.

If one looks at the resonance broadening for each nuclide and for both the capture and fission rates (see Figs. 9, 10, and 11), one notices:

- For the UOX segment:
  - At BOL: the main effect comes from the increase of the capture rate of U-238; there is also a reduction of the fission rate of U-235, which implies a stronger reduction in ηf than the effect due to U-238 only.

- At EOL: two main differences from BOL can be noticed; the first one is the production of Pu isotopes through the capture of U-238; the second one is a spectrum hardening, precisely due to these Pu isotopes (the average energy of the neutrons emitted by fission is also higher for Pu-239 and Pu-241 than for U-235). Then, the capture rates increase from BOL to EOL due to Pu-239 and Pu-240 (and even Pu-241 and U-235). But there is a significant rise in the fission reaction rates of mostly Pu-239 and also Pu-241 and U-235. This increase is so important that it contributes to a positive variation of ηf. Thus, despite the slight decrease of p, the positive contribution of ηf worsens the total Doppler coefficient (Doppler coefficient smaller at EOL than at BOL, i.e. less negative).

N.B.2: Since the increase of the fission rate is larger than the increase of the capture rate, the Doppler effect is so-called "positive" for Pu-239 (and "negative" for U-238, as the opposite behaviour is observed).

- From BOL to EOL, the shape of the Doppler coefficient can be observed in Fig. 12. Let us characterize the effect of Gd on the reactivity coefficients. When the Gd depletes, the following effects are encountered. The fast fission factor ε decreases since less thermal neutrons are captured. The resonance escape probability p increases since the probability of resonance capture in Gd decreases. And the product between the thermal fission factor and the thermal utilization factor $\eta f = \nu\Sigma_f/\Sigma_a$ increases since Σ_a decreases due to the Gd depletion. Then one has the following Fig. 7. Recall that this analysis only takes

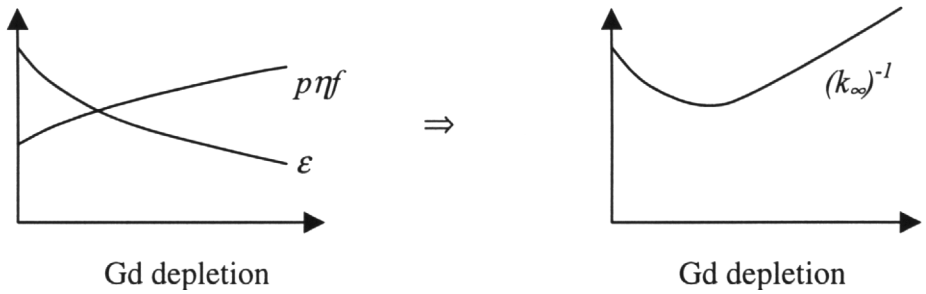

Fig. 7 Effect of the Gd Depletion on the Infinite Multiplication Factor

the Gd depletion into account. One has then to superimpose the variation of the reactivity coefficients due to the fuel depletion and one finally obtains the following Fig. 8.

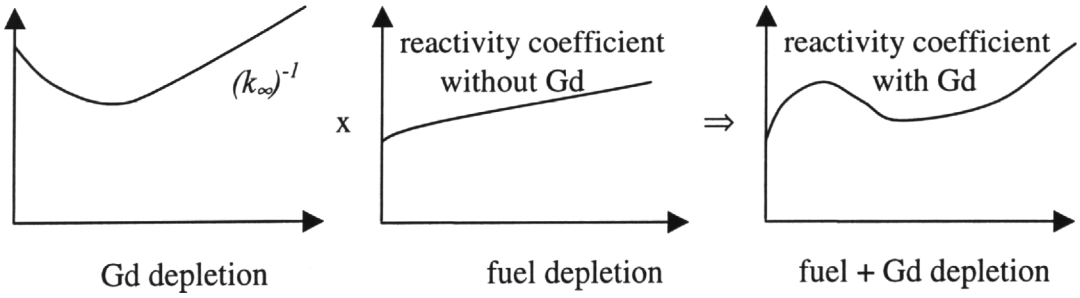

Fig. 8 Effect of the Gd Depletion on Reactivity Coefficients

    - Finally, if one increases the void fraction, the thermalization is less effective; it means that the effect of the resonance region becomes stronger. Then the variation of the resonance escape probability (due to a fuel temperature change) is more negative, which results in a more negative Doppler coefficient. It means also, as can be verified on the figures, that the capture rates variations are more significant than the fission rates variations due to a fuel temperature change, in case of spectrum hardening.
- For the MOX segment:
    - At BOL: the same explanation as the one for the UOX bundle can be held. Nevertheless, the Doppler coefficient is more negative since the variation of p is more negative. This is mostly due to Pu-240. For this nuclide, the fission rate variation is almost non-existent. Since the amount of Pu-240 is much more significant in the MOX bundle than in the UOX bundle, the increase of the capture rate of Pu-240 is not counterbalanced by any increase of the fission rate, as is the case for U-238, Pu-239 and Pu-241. Then p decreases much more significantly.
    - At EOL: the Doppler coefficient is a little bit more negative than for the UOX bundle since the effect of Pu-240 mentioned above is already sensitive at BOC. The variation of ηf is also reduced since the thermal fission factor is larger for the MOX bundle than for the UOX bundle. Then $1/\eta f$ is lower and so is its variation.
    - From BOL to EOL: see the explanation for the UOX bundle. The Gd effect is not observed for the Doppler coefficient since the Gd pins are not directly neighboring the water cells/water gaps.
    - Influence of the void fraction: see the explanation for the UOX bundle.

In summary, one can say that Pu-239 introduces a positive contribution in the Doppler coefficient because the increase of the fission rate is larger than the increase of the capture rate. In case of MOX bundles, p is more negative (strongly at BOL, slightly at EOL), because of Pu-240, the density of which is larger than for UOX bundles.

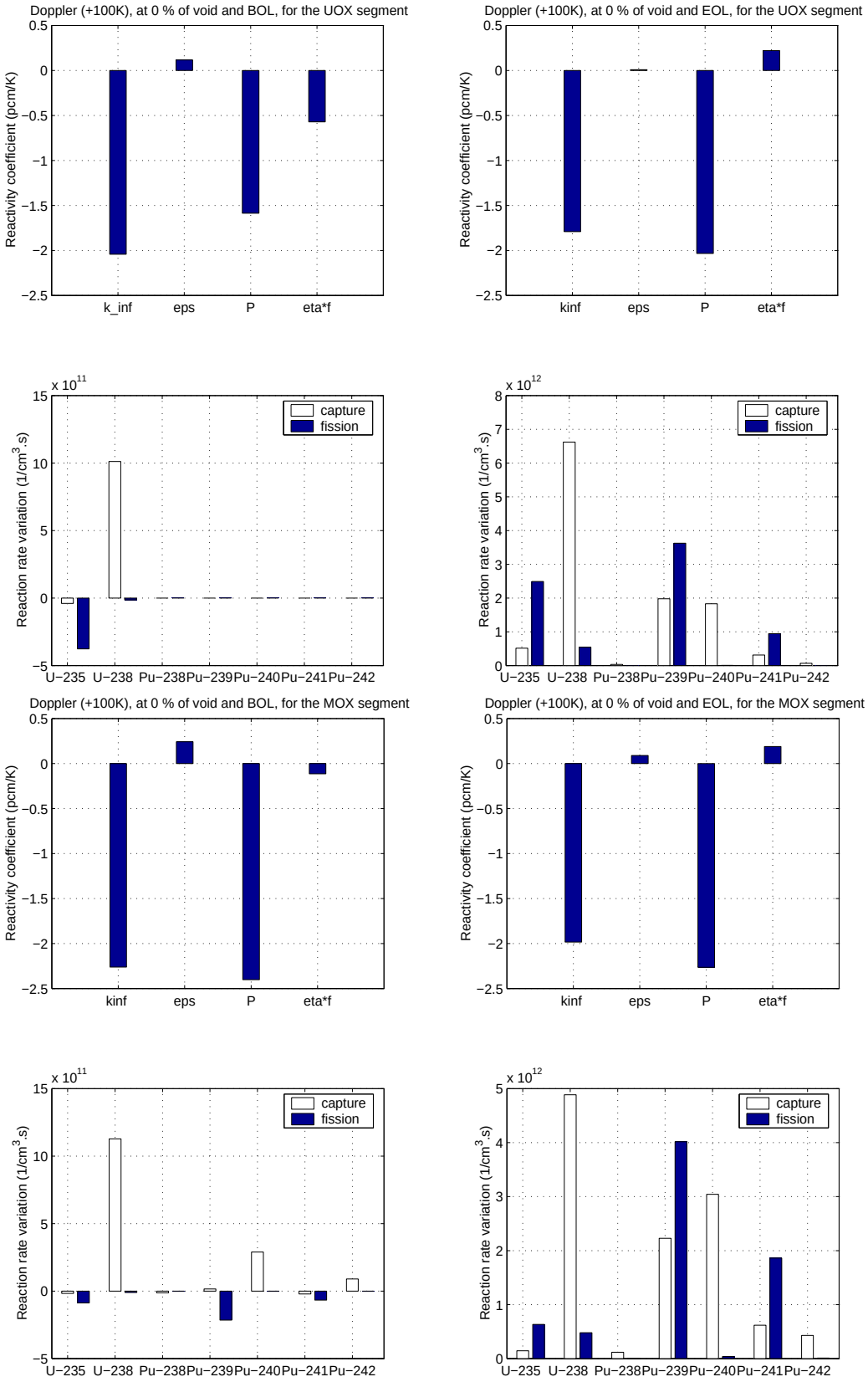

Fig. 9 Doppler Analysis at 0 % of Void

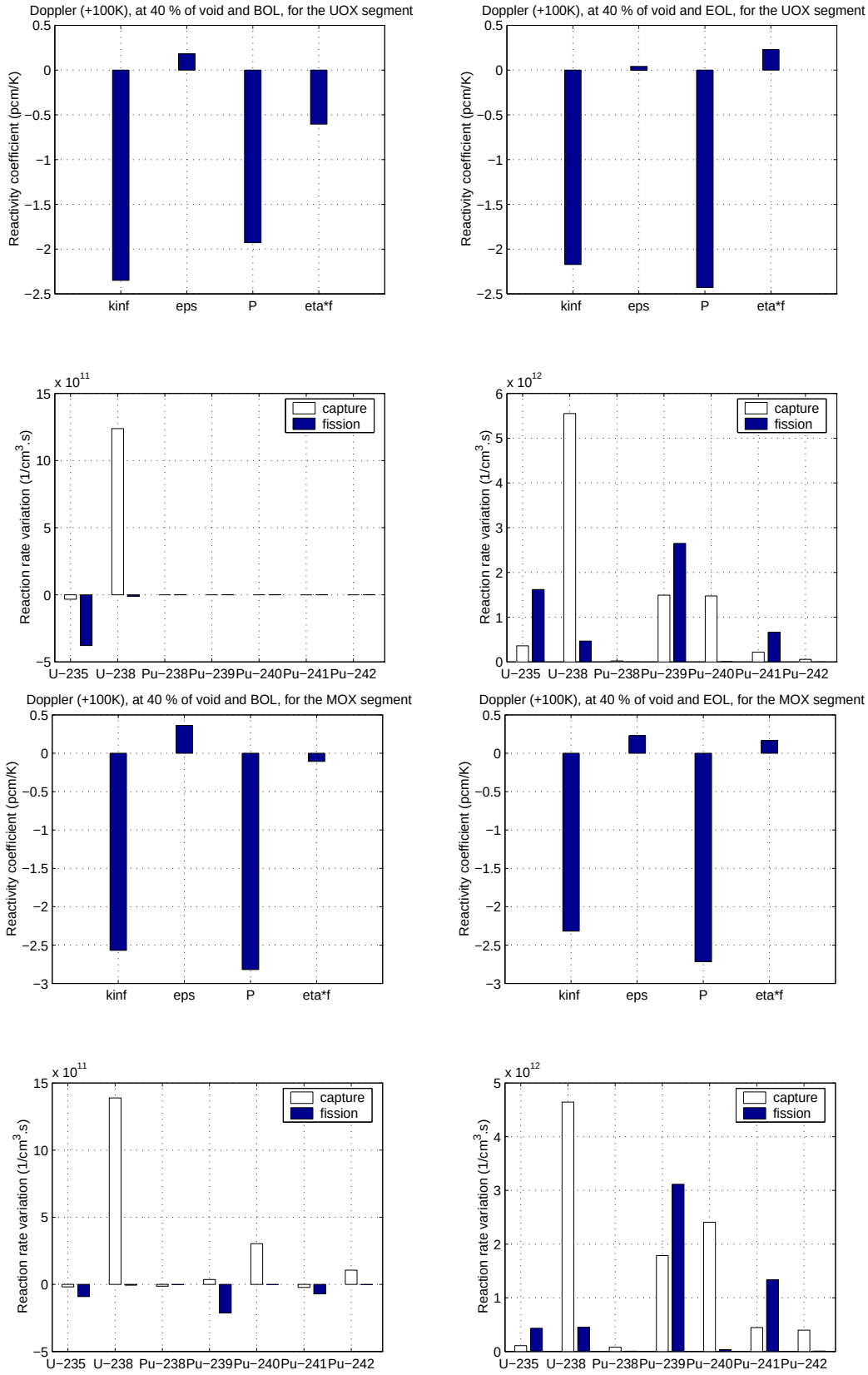

Fig. 10 Doppler Analysis at 40 % of Void

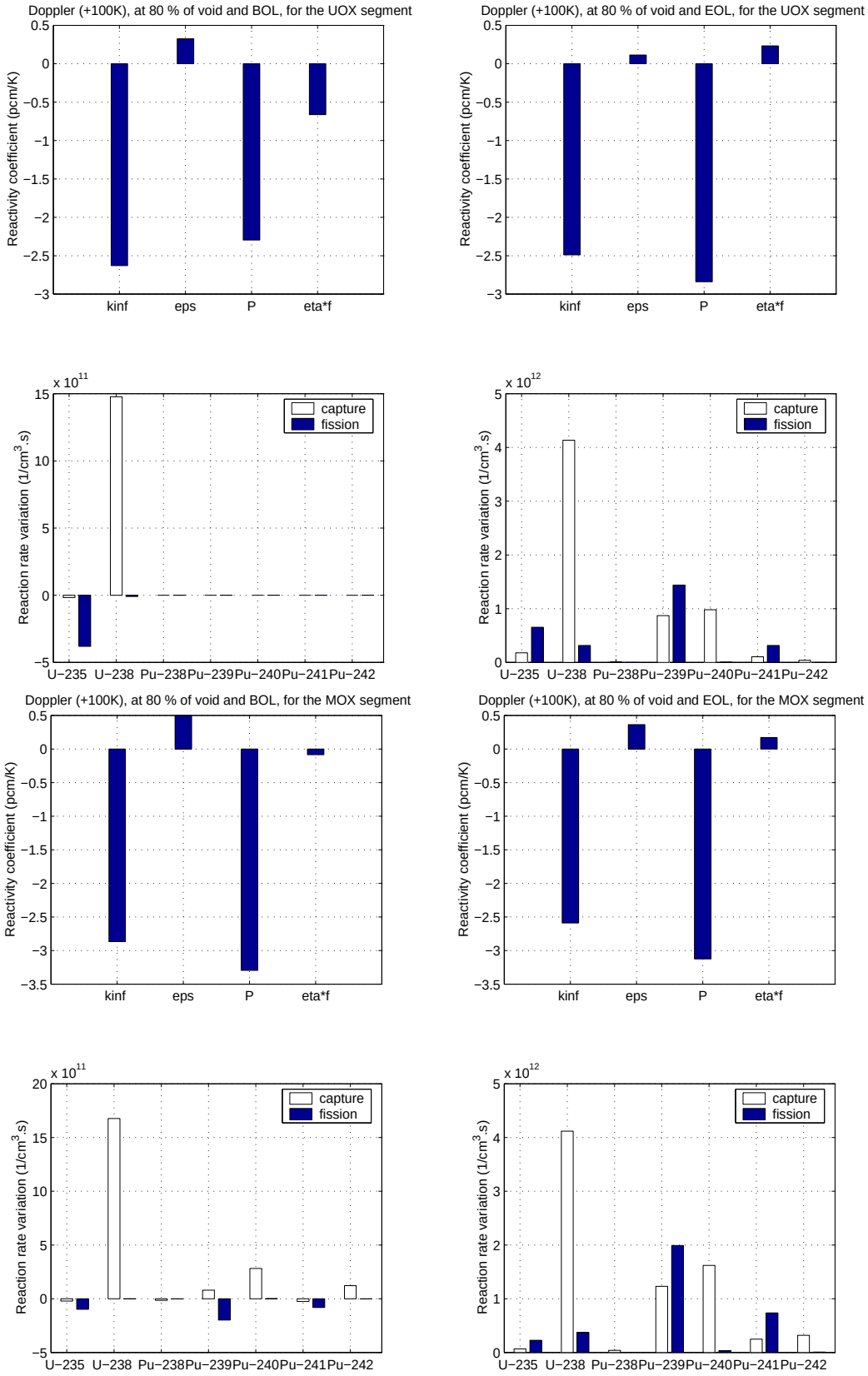

Fig. 11 Doppler Analysis at 80 % of Void

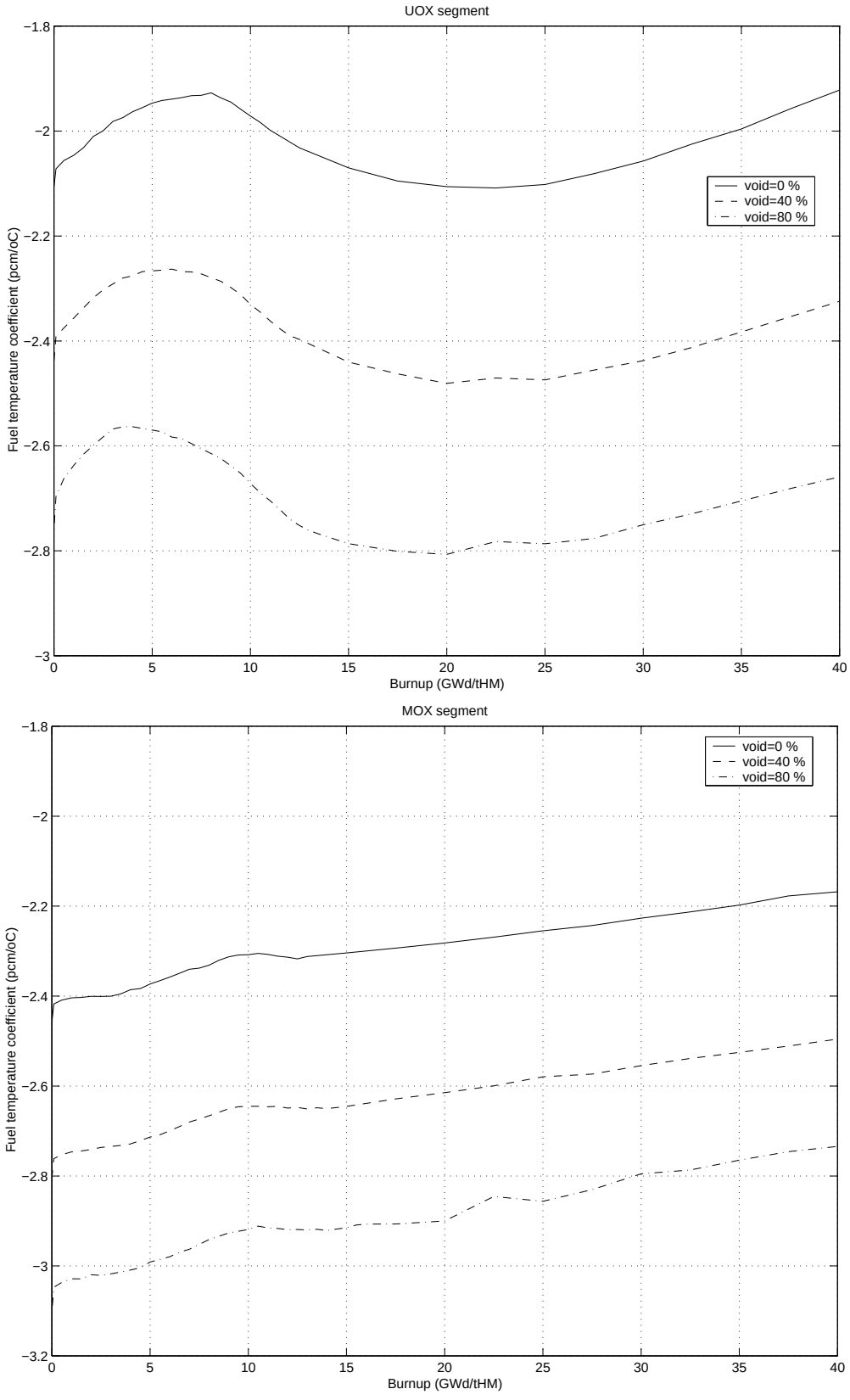

Fig. 12 Variation of the Doppler Coefficient With the Fuel Depletion

Qualitative analysis of the void coefficient

The void coefficient is the reactivity change due to a variation of void, assuming that the moderator temperature remains constant (the saturation temperature corresponding to the operating pressure). Thus only the void is varying (no temperature change). Since the lattice is undermoderated, the reactivity will decrease. However, the removal of neutron absorbing material, as in boiling, will tend to increase the reactivity. Therefore, the effect of boiling on reactivity tends to be complex. The picture becomes particularly challenging when the boiling becomes unsteady with time and thermal-hydraulic two-phase flow considerations affect the voiding.

Consequently, the increase in the production of steam bubbles or voids by boiling reduces the average density of the water in the core and also reduces the moderator to fuel ratio. This may affect the reactivity in the following ways (see reference 6):

- The reduction of the average density of the moderator causes neutron mean free paths in the core to be increased, thus increasing neutron leakage. Starting with:

$$L^2 = \frac{D}{\Sigma_a} = \frac{1}{3\Sigma_a(\Sigma_a + N_m\sigma_{s_m}(1-\bar{\mu}))} \tag{13}$$

  where $\bar{\mu}$ is the average cosine of the scattering angle, one obtains:

$$\frac{\partial L^2}{\partial \alpha} = -L^2 \times \frac{N_m\sigma_{s_m}(1-\bar{\mu})}{\Sigma_{tr}} \times \frac{1}{\rho}\frac{\partial \rho}{\partial \alpha} > 0 \tag{14}$$

  where ρ and α denote the moderator density and the void fraction respectively, and consequently:

$$-\frac{B^2}{1+L^2B^2}\frac{\partial L^2}{\partial \alpha} < 0$$

  This is a negative reactivity effect.

- The reduction in the moderator to fuel ratio increases the fraction of neutrons captured in the resonances during the slowing-down. From Eq. (11), one concludes:

$$\frac{1}{p}\frac{\partial p}{\partial \alpha} = -\ln p \times \frac{1}{N_m}\frac{\partial N_m}{\partial \alpha} < 0 \tag{15}$$

  This is a negative reactivity effect.

- The reduction in the moderator to fuel ratio reduces the fraction of thermal neutrons captured in the moderator and the thermal utilization factor increases. From:

$$f = \frac{V_f\Sigma_{a_f}\Phi_f}{V_f\Sigma_{a_f}\Phi_f + V_m\Sigma_{a_{fm}}\Phi_m} \tag{16}$$

  one deduces that:

$$\frac{1}{f}\frac{\partial f}{\partial \alpha} = (f-1) \times \frac{1}{N_m}\frac{\partial N_m}{\partial \alpha} > 0 \tag{17}$$

This is a positive reactivity effect.

- The reduction in the moderator to fuel ratio increases the age, since the number of neutrons captured in the resonances during the slowing-down increases. The age is defined as:

$$d\tau = \frac{D(u)}{\xi\Sigma_s(u)}du \Leftrightarrow \tau_{th} = \int_{u_0}^{u_{th}} \frac{D(u)}{\xi\Sigma_s(u)}du \tag{18}$$

where u is the lethargy and the subscript *th* denotes the thermal energy. Assuming that $D/\xi\Sigma_s$ is relatively independent of the lethargy and choosing the origin of the lethargy such as $u_0 = 0$, one finally obtains:

$$\frac{1}{\tau_{th}}\frac{\partial\tau_{th}}{\partial\alpha} = -\frac{\Sigma_a + 2N_m\sigma_{s_m}(1-\bar{\mu})}{\Sigma_a + N_m\sigma_{s_m}(1-\bar{\mu})} \times \frac{1}{N_m}\frac{\partial N_m}{\partial\alpha} > 0 \tag{19}$$

and consequently: $-B^2\frac{\partial\tau}{\partial\alpha} < 0$.

This is a negative reactivity effect.

- The reduction in the moderator to fuel ratio increases the flux around the fission energies and the fast fission factor increases. This can be explained by the fact that the probability of collision with the moderator molecules is smaller compared with the collision with heavy nuclei and also by the increase of the flux, as explained below.
Let us define the slowing-down (density) operator as follows (in the isotropic case) for the nuclide *i*:

$$\rho_i(u) = \int_{u-\varepsilon_i}^{u} \Sigma_{s,i}(u')\Phi(u')\frac{e^{-(u-u')}}{1-\alpha_i}du' \tag{20}$$

where:
  - $\alpha_i = \left(\frac{A_i - 1}{A_i + 1}\right)^2$ with A_i designating the mass of the nuclide *i*;
  - $\varepsilon_i = -\ln\alpha_i$ is the maximum lethargy gain per collision with nuclide *i*.

If one assumes that the slowing-down by heavy nuclei is negligible, this operator can be regarded as a constant (the integration interval is always much larger than the resonance width, so that the integration flattens the variation of the function): $\rho_m(u)$ does not present strong variations and a good approximation is given by $\rho_m(u) = C = \Sigma_t(u)\Phi(u)$. The constant can be eliminated by the use of the asymptotic flux as follows:

$$\rho_m(u) = \Sigma_t(u)\Phi(u) = C = \Sigma_{t_{as}}\Phi_{as} \tag{21}$$

where $\Phi_{as} = \frac{q_{as}}{\xi\Sigma_s}$ and $\Sigma_{t_{as}} = \Sigma_{s_{as}}$, and one finally obtains:

$$\Phi(u) = \frac{q_{as}}{\xi} \times \frac{1}{\Sigma_a(u) + N_m\sigma_{s_m}(u)} \tag{22}$$

Consequently, since $\partial N_m / \partial \alpha < 0$, the flux increases. This flux increase, combined with the increase of the probability of collision with heavy nuclei, gives an increase of ε, so that: $1/\varepsilon \times \partial\varepsilon/\partial\alpha > 0$.

This is a positive reactivity effect.

N.B.: There is no significant change in the thermal fission factor η with the void content.

If one looks at the void increase and its consequences on each nuclide and for both the capture and fission rates (see Figs. 13, 14, and 15), one notices:

- For the UOX segment:
  - At BOL: the increase of the fast fission factor is significant since both the U-235 fission rate decreases and the U-238 fission rate increases. The strong increase of the capture rate of U-238 gives a significant variation of the resonance escape probability. As expected, the thermal utilization factor increases.
  - At EOL: the Pu build-up gives a spectrum hardening. Then the capture rates increase slightly from BOL to EOL due to U-238, Pu-239, and Pu-240. The variation of ε is less significant than the one at BOL, since the number of thermal fissions is increased by the thermal fissions of Pu-239 and Pu-241. The magnitude of the η*f* variation ($1/\eta f \times \partial \eta f / \partial \alpha$) is increased since *f* is lowered from BOL to EOL: the macroscopic absorption cross-section $\Sigma_{a_{fuel}}$ decreases from BOL to EOL due to the consumption of U-235 (the Pu build-up through U-238 cannot compensate for this decrease since the mass proportions of the Pu isotopes are significantly lower than the initial mass proportion of U-235 in the fuel).
  - From BOL to EOL: the void coefficient decreases since the decrease of the ε variation is stronger than the increase of the η*f* variation. The “wave” shape that can be observed (see Fig. 16) is due to the Gd depletion described beforehand.
  - Finally, if one increases the void fraction, the thermalization is less effective and the effect of the resonance region becomes much stronger. Then the change in the resonance escape probability is more negative. For the same reason, this spectrum hardening strengthens the effect on the fast fission factor, for which the change becomes more positive. Nevertheless, the effect on *p* is more predominant than the one on ε, so that the void coefficient is more negative.
- For the MOX segment:
  - At BOL: since the Pu isotopes are already present at BOL, the spectrum is hardened in comparison with the UOX bundle. Thus the previous analysis can be held: the change in *p* is more negative and the change in ε is more positive, but the effect on *p* is more significant than the one on ε, so that the void coefficient is lowered. This is reinforced by the change in η*f*, which is less strong. This is the result of a macroscopic absorption cross-section larger than the one in the corresponding UOX bundle.
  - At EOL: the change in η*f* is increased since, as the UOX bundle, the macroscopic absorption cross-section decreases (only due to the depletion of the Pu isotopes this time, Pu-239 mostly). For ε and *p*, the same analysis as the one held for the UOX bundle can be followed.
  - From BOL to EOL: see the explanation for the UOX bundle.
  - Influence of the void fraction: see the explanation for the UOX bundle.

In summary, one can say that in case of MOX fuel, the harder spectrum gives an increase in the change in the capture rates, so that the variation of p becomes more negative. For the same reason, this spectrum hardening strengthens the changes in the fast fissions, so that ε becomes more positive. Nevertheless, the effect on p is more significant than the one on ε, and consequently the void coefficient is lowered (more negative). This is reinforced by the change in ηf, which is less strong (f is larger since the macroscopic absorption cross-section is larger than the one of the corresponding UOX bundle).

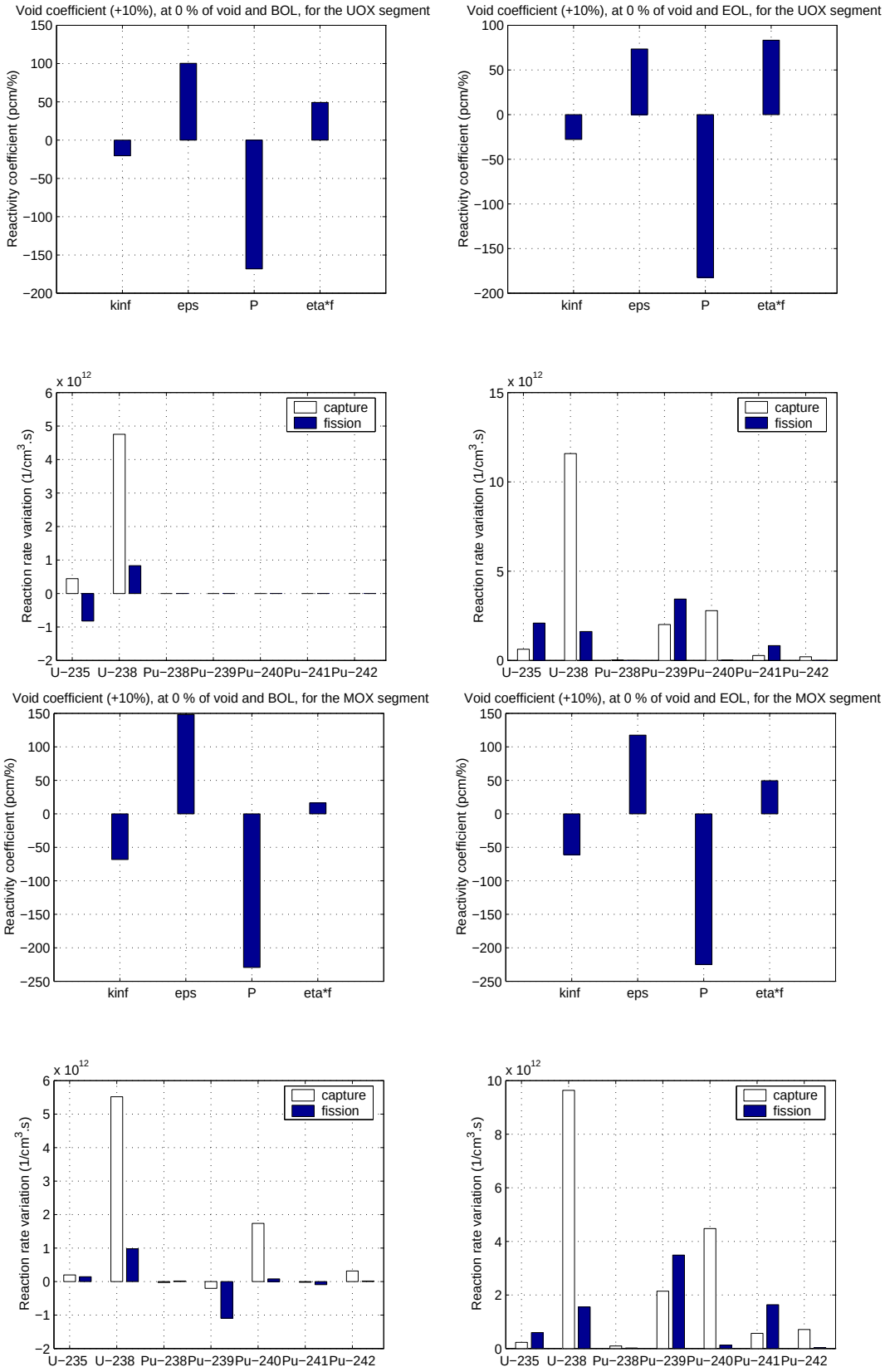

Fig. 13 Void Coefficient Analysis at 0 % of Void

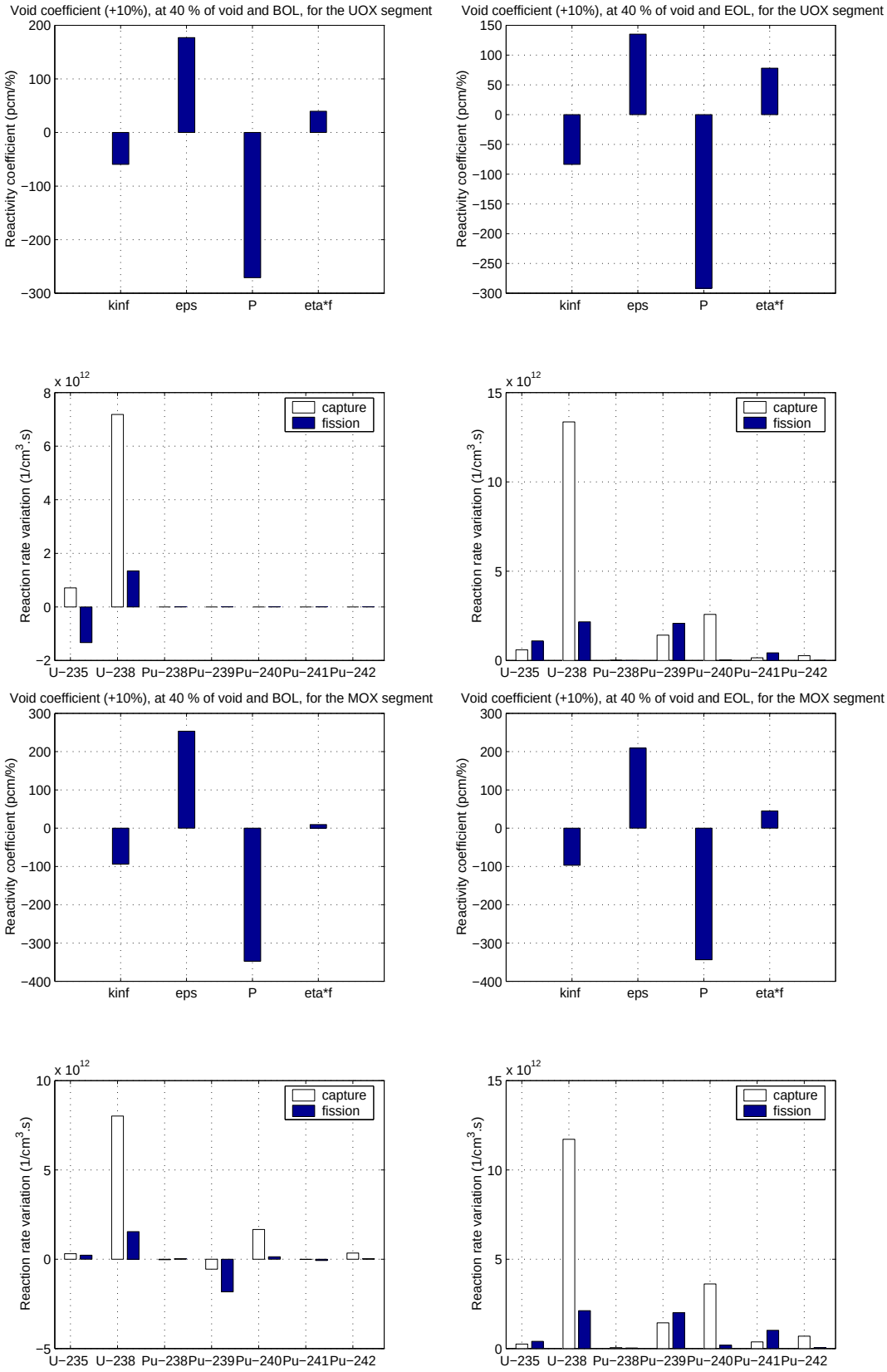

Fig. 14 Void Coefficient Analysis at 40 % of Void

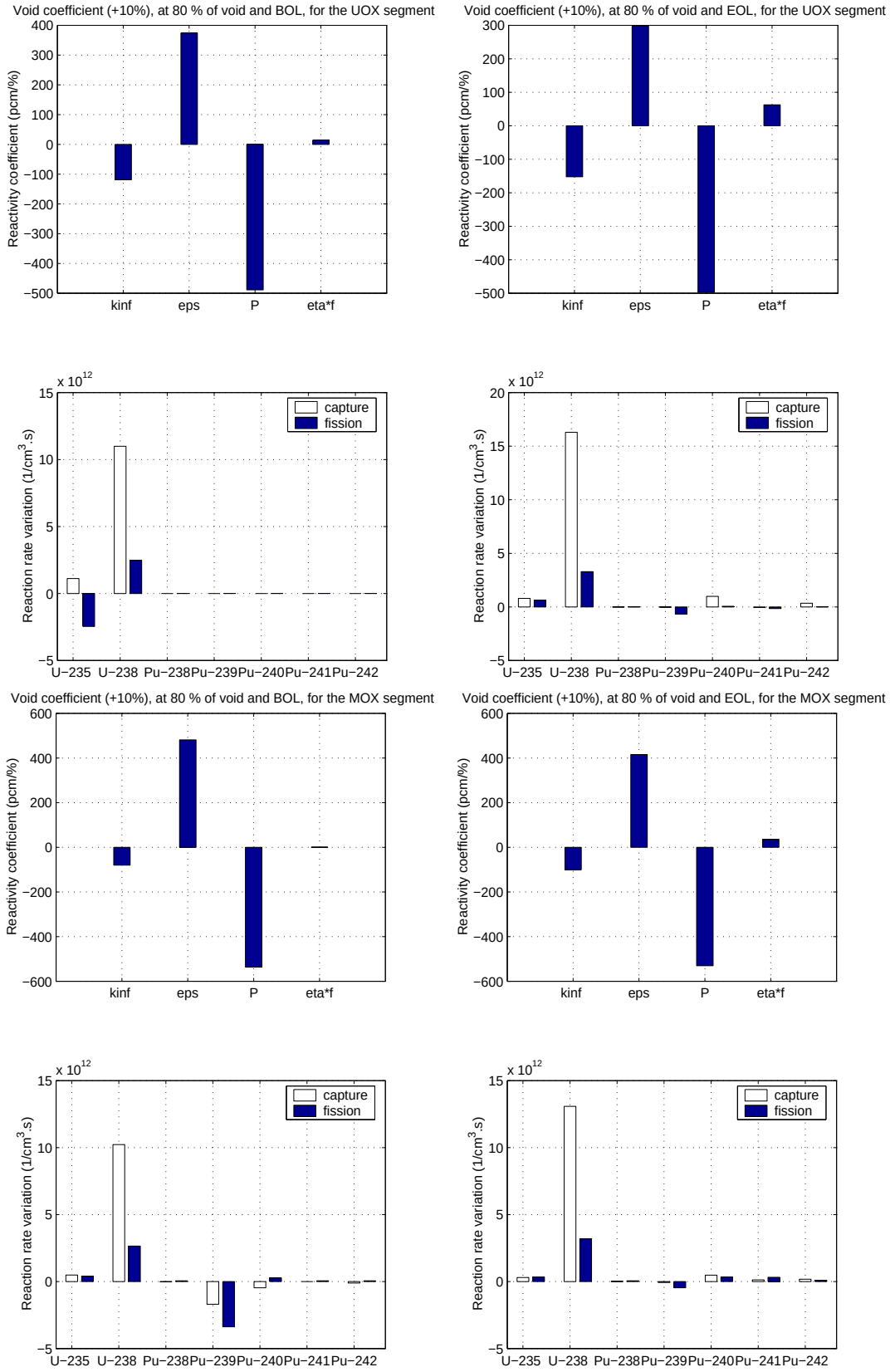

Fig. 15 Void Coefficient Analysis at 80 % of Void

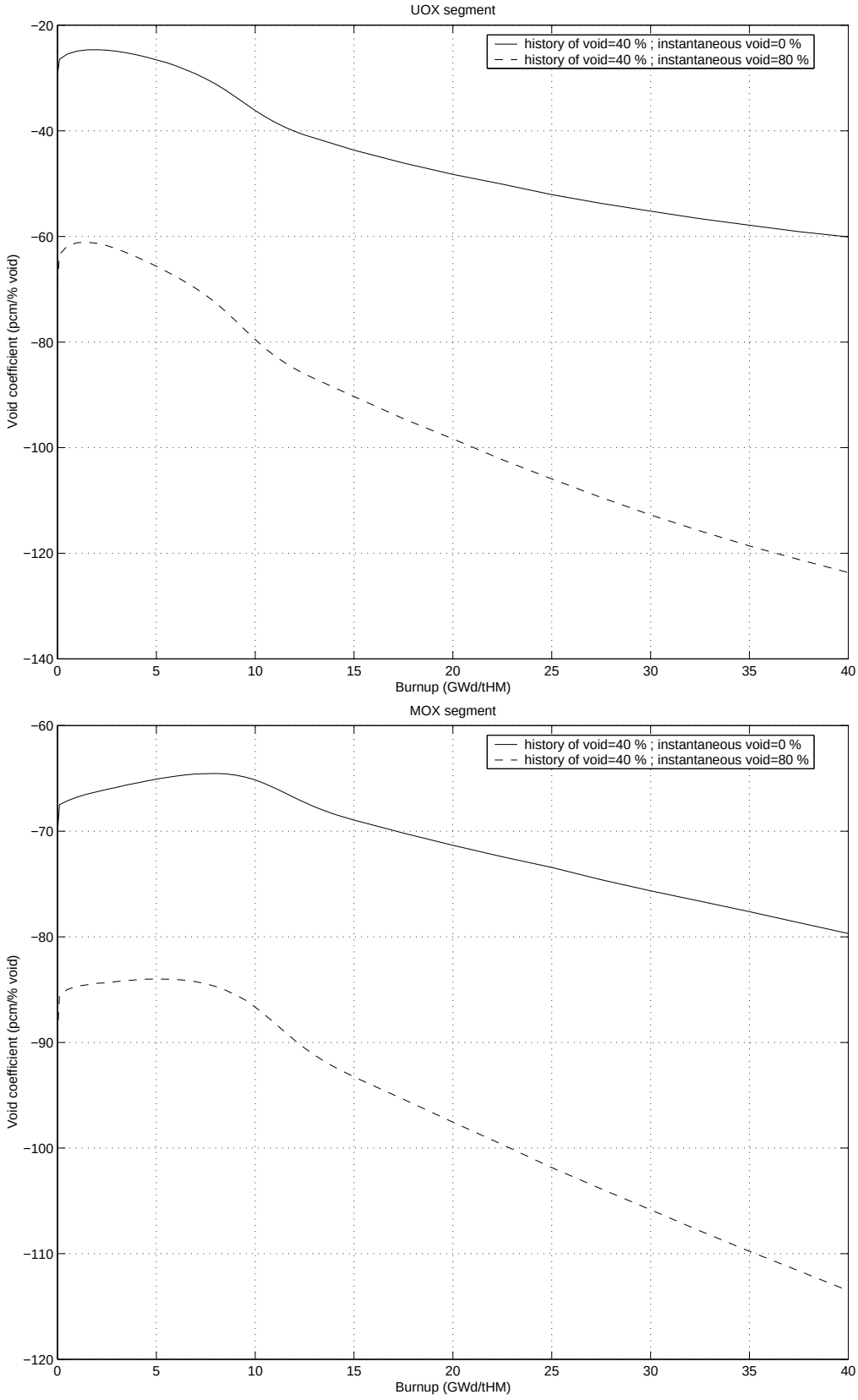

Fig. 16 Variation of the Void Coefficient With the Fuel Depletion

Quantitative analysis:

In the previous paragraphs, the reactivity coefficients have been calculated for each bundle via CASMO-4. In this section, one will present the reactivity coefficients that describe the whole core via SIMULATE-3. As a matter of fact, CASMO-4 only gives a kind of contribution to the studied reactivity coefficients due to a peculiar bundle, whereas SIMULATE-3 allows studying the reactivity coefficients for the whole core.

This is why the quantitative analysis is based on the SIMULATE-3 results mostly. The following Table VII summarizes the main results for the full UOX core, the base mixed UOX/MOX core, and the full MOX core.

Table VII: Summary of the Reactivity Coefficients and the Associated Parameters

Parameters	Full UOX core		Base UOX/MOX core		Full MOX core	
	BOC	EOC	BOC	EOC	BOC	EOC
MTC[a] (pcm/F)	-55,44	-57,01	-57,69	-60,37	-64,46	-62,84
UDP[b] (pcm/F)	-1,12	-1,08	-1,10	-1,15	-1,19	-1,16
POW[c] (pcm/%power)	-41,80	-45,81	-42,66	-47,37	-45,52	-46,85
FLO[d] (pcm/%flow)	31,63	36,57	32,53	37,66	34,72	37,22
PRE[e] (pcm/psia)	9,32	8,43	7,96	8,82	8,78	9,00
β_{eff} [f] (pcm)	604	532	536	491	408	417
Λ [g] (μs)	39,6	41,4	34,1	35,9	24,5	26,5
CR worth[h] (pcm)	35023	35965	32132	33251	26854	28164
SDM[i] (%)	2,426	3,756	0,737	3,039	0,705	2,343

a. The Moderator Temperature Coefficient is the reactivity change associated with a change in the moderator inlet temperature divided by the change in the inlet moderator temperature.

b. The Uniform DoPler coefficient is the reactivity change associated with a uniform change in the fuel temperature divided by the change in the averaged fuel temperature.

c. The POWer coefficient is the reactivity change associated with a uniform change in the power level divided by the percent change in power (the power distribution used to evaluate the cross-sections is unchanged).

d. The FLOw coefficient is the reactivity change associated with a uniform perturbation of the flow density divided by the percent change in flow.

e. The PREssure coefficient is the reactivity change associated with a perturbation of the primary system pressure divided by the pressure change.

f. Effective fractional yield of delayed neutrons per fission neutron.

g. Prompt neutron lifetime.

h. The Control Rod worth is the total worth of the whole control bank.

i. The cold ShutDown Margin is the instantaneous amount of reactivity by which the reactor is subcritical assuming all control rods are fully inserted except for the most reactive control rod which is fully withdrawn.

In summary, one can say that the uniform Doppler coefficient (UDP) is almost unchanged in case of MOX bundles, whereas the void coefficient (most of the MTC) is more negative, as expected. The power coefficient (POW) is slightly larger (more negative), and so is the flow coefficient (FLO) (more positive). The pressure coefficient (PRE) is also slightly smaller at BOC, but larger at EOC.

The most significant changes are the variation of the effective fraction (β_{eff}) of delayed neutrons (due to Pu-239 and Pu-240, 210 pcm and 490 pcm respectively, in comparison with U-235, 650 pcm), the variation of the prompt neutron lifetime (Λ), and the reduction of the control rod efficiency. This reduction is so strong that the shutdown margin (SDM) becomes smaller than 1 % at BOC. The high value for the thermal absorption cross-section of the MOX fuel causes a reduction in the mean free path of thermal neutrons, which reduces the thermal neutron absorption probability for the control rod.

It was also decided, for the UOX/MOX core exclusively, to model a variation of the Pu isotopic vector in order to study the evolution of the previous parameters. A variation of ± 50 % of each Pu isotope (relative to their nominal value) was carried out. A variation of the Pu-2*xx* isotope is referenced as m*xx* and p*xx*, for -50 % and +50 % of variation respectively. All the absolute results are given, and also their variation:

- relative to the full UOX core, for the UOX/MOX core and the full MOX core;
- relative to the nominal UOX/MOX core, for a Pu isotopic vector variation.

Regarding the variation of the Pu quality, one could notice that there is no significant change with the Pu isotopic vector (only a significant reduction of Pu-239 gives a decrease of the power coefficient) except for the shutdown margin (see Fig. 17). The SDM can become greater than 1 % if one reduces the Pu-239 amount and/or one increases the Pu-240 amount. This is the result of the large absorption cross-section of Pu-239 (≈ 1035 barn in the thermal region), whereas the Pu-240 absorption cross-section is relatively small (≈ 197 barn in the thermal region). Consequently, any reduction in the absorption cross-section tends to increase the control rod efficiency, as explained beforehand. The influence of the other Pu isotopes is less significant, since their nominal proportion is relatively small compared with Pu-239 and Pu-240.

4.2 STABILITY ANALYSIS

As mentioned earlier, no dynamic code is yet available at the Department of Reactor Physics, Chalmers University of Technology. Consequently, it was decided to use a “simple” qualitative model that allows studying the stability of BWRs. This model is the March-Leuba model (see reference 7).

Before using this model, let us define the different kinds of instabilities that can occur in a BWR. This presentation is based on references 8 and 9. Three main modes of instability may exist in a BWR:

- the fundamental mode or in-phase oscillation, in which the fundamental flux is oscillating over the whole core;

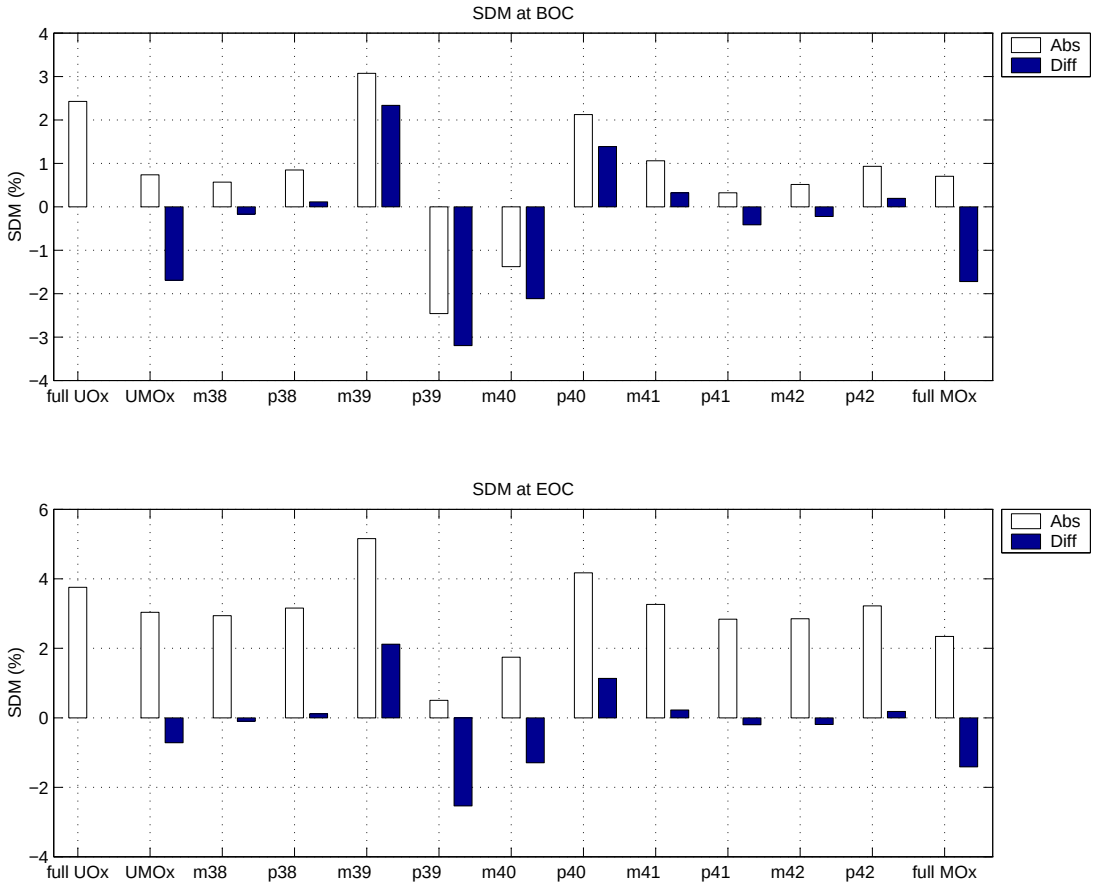

Fig. 17 Analysis of the Shutdown Margin

- the first azimuthal mode or out-of-phase oscillation, in which the first azimuthal flux is oscillating over the whole core.
- the channel instability or density wave oscillation, in which the flux is oscillating only in a certain channel.

The two first ones are caused by the time delay of the void/pressure response due to any reactivity perturbation: in some cases, the initial perturbation can be reinforced by the void/pressure feedback if the phase of this delayed response coincides with the phase of the reactivity perturbation. This is called the direct loop. Because of the outlet pressure variation, the initial reactivity perturbation induces also a core inlet flow perturbation, through the recirculation loop. This flow variation creates consequently a void response, and so on. This loop is thus called indirect loop. But the effect of this indirect loop is smaller than the direct loop since the flow oscillations are damped by the friction in the recirculation loop.

Nevertheless, the indirect loop may become a source of channel instability. For such an instability, only a single bundle (and its neighboring assemblies to some extent) are concerned by a purely thermal-hydraulic feedback effect (the reactivity feedback is not responsible for the coupling). This instability is induced by an inlet flow rate perturbation. Due to the consecutive void response and the time delay for this response to travel along the bundle (density wave), the corresponding pressure drop at the channel outlet could enhance the inlet flow rate perturbation, through the

recirculation loop.

In the March-Leuba model, only the direct loop is taken into account, which means that the density perturbation (variation of the flow rate) cannot be represented, i.e. the indirect loop mechanism is ignored. It could have been possible to model the density perturbation (see reference 8), but one would have obtained a complicated additional term with derivatives of the channel inlet mass flow, which must be calculated separately by the recirculation loop equation. Furthermore, except for the density wave oscillations in which the indirect loop is responsible for the instability, only the direct loop can be considered with a good approximation, since the flow oscillations are damped by the friction in the recirculation loop.

The March-Leuba stability model can then be described as:

$$\frac{\partial \delta n}{\partial t}(t) = \frac{\rho_0 - \beta_{eff}}{\Lambda}\delta n(t) + \lambda \delta c(t) + \frac{\delta\rho_p(t) + \delta\rho_r(t)}{\Lambda} n_0 \tag{23}$$

$$\frac{\partial \delta c}{\partial t}(t) = \frac{\beta_{eff}}{\Lambda}\delta n(t) - \lambda \delta c(t) \tag{24}$$

$$\frac{\partial \delta \bar{T}_f}{\partial t}(t) = a_1 \frac{\delta \bar{q}(t)}{\bar{q}_0} - a_2 \delta \bar{T}_f(t) \tag{25}$$

$$\frac{\partial^2 \delta\rho_\alpha}{\partial t^2}(t) + \frac{6}{\tau}\frac{\partial \delta\rho_\alpha}{\partial t}(t) + \frac{12}{\tau^2}\delta\rho_\alpha(t) = \frac{CH^2}{\tau}\left[\frac{\partial \delta \bar{T}_f}{\partial t}(t) + \frac{6}{\tau}\delta \bar{T}_f(t)\right] \tag{26}$$

$$\delta\rho_r(t) = \delta\rho_\alpha(t) + D\delta \bar{T}_f(t) \tag{27}$$

The two first equations are the point-kinetic equations, in which $n(t)$, $c(t)$, ρ_0, $\delta\rho_p(t)$, and $\delta\rho_r(t)$ denote the neutron density, the precursor density, the initial reactivity, the perturbed reactivity, and the feedback reactivity respectively. The third equation is the Doppler reactivity feedback, in which $\bar{T}_f$, and $\bar{q}$ are the average fuel temperature, and the average power density respectively (a_1 and a_2 are two coefficients). The fourth equation is the void reactivity feedback, after the use of the Padé-approximation (for $x = s\tau << 1$):

$$\exp(-x) \approx \frac{1 - \frac{x}{2} + \frac{x^2}{12}}{1 + \frac{x}{2} + \frac{x^2}{12}} \tag{28}$$

H is the channel height, C and τ are two coefficients, and $\delta\rho_\alpha(t)$ is the reactivity due to the void. The fifth equation expresses that the reactivity feedback is only constituted by the void and the Doppler reactivity feedback, where D represents the Doppler reactivity coefficient.

If the variations are defined relative to their initial stationary state and normalized to them, the Laplace-transform allows calculating the transfer function of the reactor (from reactivity perturbation to normalized neutron density variation):

$$H(s) = \frac{\delta N(s)}{\delta \rho_p(s)} \tag{29}$$

$$= \frac{\left(s^2 + s\frac{6}{\tau} + \frac{12}{\tau^2}\right)(s + a_2)}{\Lambda\left(s + \frac{\beta_{eff}}{\Lambda}\right)(s + a_2)\left(s^2 + s\frac{6}{\tau} + \frac{12}{\tau^2}\right) - a_1\left[D\left(s^2 + s\frac{6}{\tau} + \frac{12}{\tau^2}\right) + \frac{CH^2}{\tau}\left(s + \frac{6}{\tau}\right)\right]}$$

This transfer function has been obtained by neglecting the precursor decay constant $\lambda << s$ (with $\rho_0=0$), since the driving mechanism of feedback is mainly the void reactivity feedback. The dynamics must reflect the bubble residence time τ, so $1/\tau$ is the frequency region of interest. In such a region $\lambda << s$. The denominator of $H(s)$ is a fourth-order polynomial, which has two real poles, and a complex pair of poles. Only this pair of complex poles is meaningful for the study of oscillating systems. It is thus assumed that the reactor behaviour can be fitted to a second order model with a transfer function of the form:

$$\tilde{H}(s) = \frac{1}{(s-\gamma)(s-\gamma^*)} \tag{30}$$

where γ is the (dominant) pole of the system and γ^* its complex conjugate. From this transfer function, it is possible to calculate the Decay Ratio (DR), defined as the ratio between two consecutive maxima of the impulse response of the normalized neutron density (the DR gives a measurement of the damping of the system) (see reference 10):

$$DR = \exp\left(\frac{2\pi \times Re(\gamma)}{Im(\gamma)}\right) \tag{31}$$

In order to understand the behaviour of the DR, an analysis of the influence of the following parameters was performed (variation relative to the nominal values corresponding to the full UOx core at EOC) (see Figs. 18 to 25):

- a_1: an increase of a_1 destabilizes the core since a_1 is an amplification factor of the fuel temperature response to a power change:

$$\delta\bar{T}_f(s) = \frac{a_1}{s + a_2}\frac{\delta\bar{q}(s)}{\bar{q}_0} \tag{32}$$

  This increases of course the Doppler response but much more the void response (this is why it is a destabilizing effect - see below). The Doppler coefficient is negligible in comparison with the void coefficient because the reactivity response for the Doppler:

$$\frac{Da_1}{a_2}\frac{\delta\bar{q}}{\bar{q}_0} \tag{33}$$

  is much smaller than the reactivity response for the void:

$$\frac{CH^2}{2}\frac{a_1}{a_2}\frac{\delta\bar{q}}{\bar{q}_0} \tag{34}$$

in case of a step increase of the power.

- a_2: the stability of the system is nearly insensitive to a_2 for several reasons:
  - a_2 represents the delay of the fuel temperature response, which is in any case very short;
  - the stability of the system is not governed by the fuel temperature feedback, but by the void reactivity feedback;
  - since the delayed response of the void, due to a fuel temperature change, is much larger than the delay of the fuel temperature response due to a power change, the delayed response of the void to a power perturbation is unchanged.

  Consequently, the DR decreases only slightly when a_2 increases, since the fuel temperature response is a little bit more rapid.
- β_{eff}: the DR increases when the effective fraction of delayed neutron β_{eff} decreases. This is entirely due to the neutronic properties of the fuel and not the thermal-hydraulic characteristics: if β_{eff} decreases, one approaches the possibility of the prompt criticality of the core, thus increasing the DR.
- C: a larger C value (more negative) destabilizes the core since the void response is a large delayed response; there is the possibility that an instability may occur. The reason is that, during the time required for the delayed feedback to become effective, the imposed reactivity perturbation may change sign. Hence it is possible for the feedback reactivity to be in phase with the imposed reactivity, thus enhancing the perturbation (the Doppler response can be neglected in comparison with the void response - see above).
- λ: the DR is fully independent of λ, since as already mentioned, $s>>\lambda$ in the frequency region of interest. Thus λ disappears from the transfer function of the system. It means also than one can neglect the delayed neutrons.
- Λ: the DR is almost insensitive to Λ since the prompt-jump approximation (or zero prompt-neutron lifetime) can be held. The point-kinetics equation, if one neglects the delayed neutrons (see above) is reduced to:

$$\Lambda\frac{\partial\delta N}{\partial t}(t) \approx (\rho_0 - \beta_{eff})\delta N(t) + (\rho_p(t) + \rho_r(t)) \tag{35}$$

  As long as one is far from prompt criticality, $\Lambda \times \partial\delta N(t)/\partial t$ is negligible and $(\rho_0 - \beta_{eff})\delta N(t) \approx -(\rho_p(t) + \rho_r(t))$. Thus $\delta N(t)$ follows $\rho_p(t) + \rho_r(t)$ (prompt jump) and Λ can be moved out from the transfer function. This is why the DR is almost insensitive to Λ (the DR increases very slightly with Λ since without the prompt-jump approximation, but without reactivity feedback and delayed neutrons, the transfer function can be approximated by $H(s) \approx (1/\Lambda)/(s + \beta_{eff}/\Lambda)$ and $1/\Lambda$ is an amplification factor of the response).
- τ: the DR increases when τ increases. This is due to the fact that τ is approximately the residence time of steam bubbles in the channel:

$$\tau = \frac{H}{\bar{V}_0} \tag{36}$$

  where $\bar{V}_0$ is the average flow velocity. If τ increases, $\bar{V}_0$ decreases (void perturbation propagation), which means that the rated core flow decreases. Consequently, the void fraction

is higher and one knows (see the analysis of the void coefficient § 4.1) that the void coefficient is larger (more negative) when the void content is larger. This is why it is a destabilizing effect.

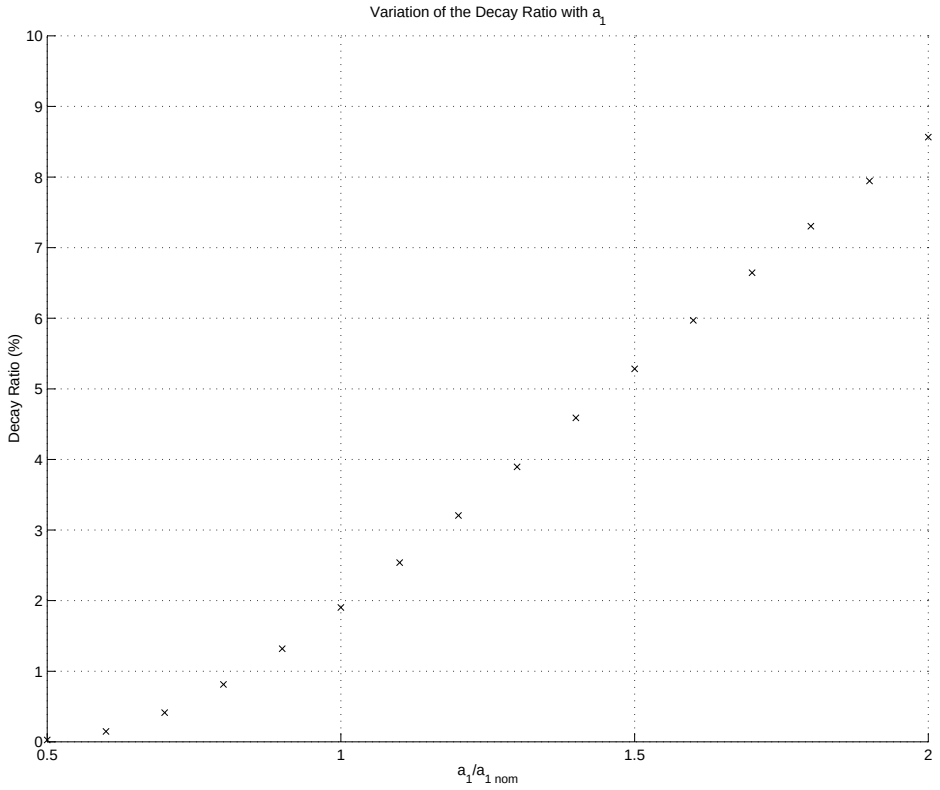

Fig. 18 Analysis of the Effect of a_1 on Stability

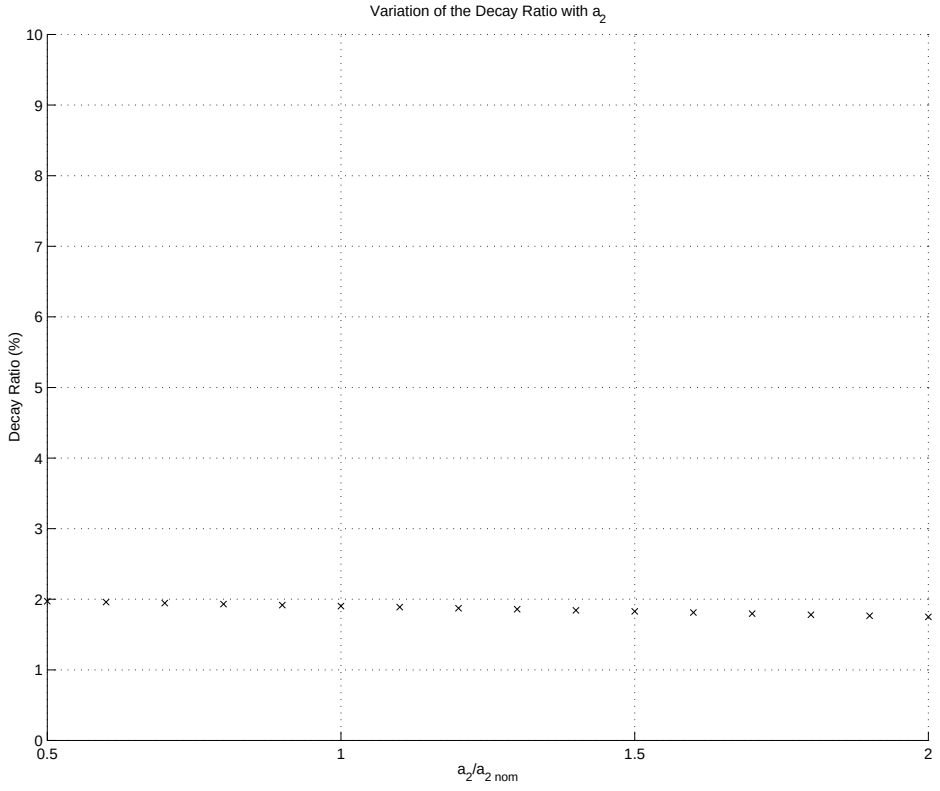

Fig. 19 Analysis of the Effect of a_2 on Stability

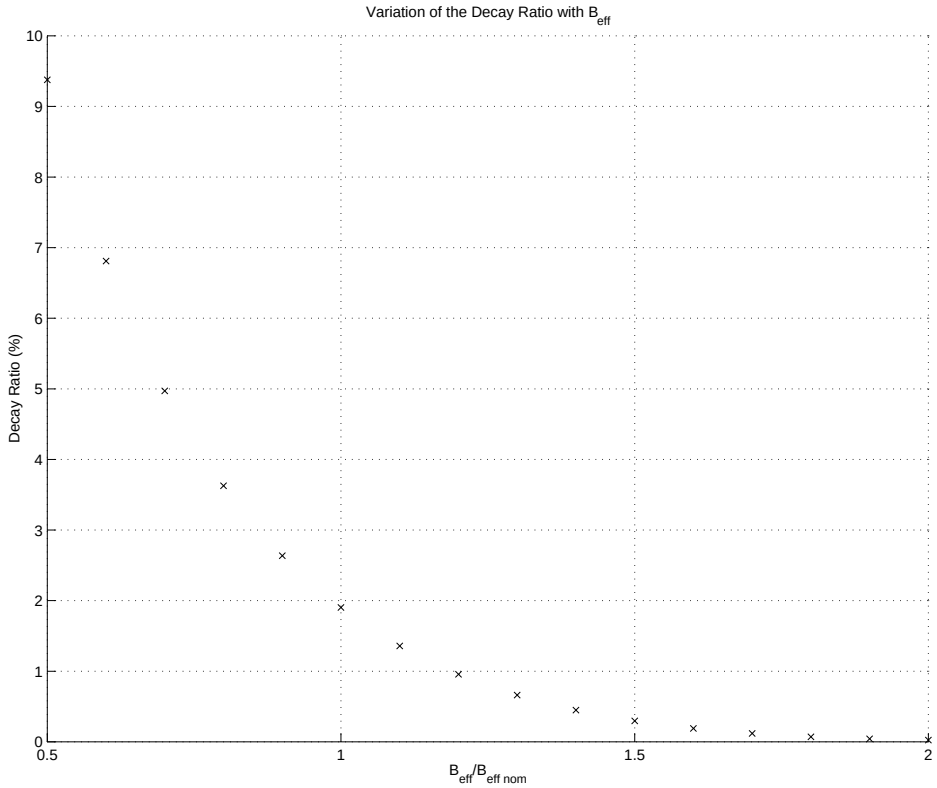

Fig. 20 Analysis of the Effect of β_{eff} on Stability

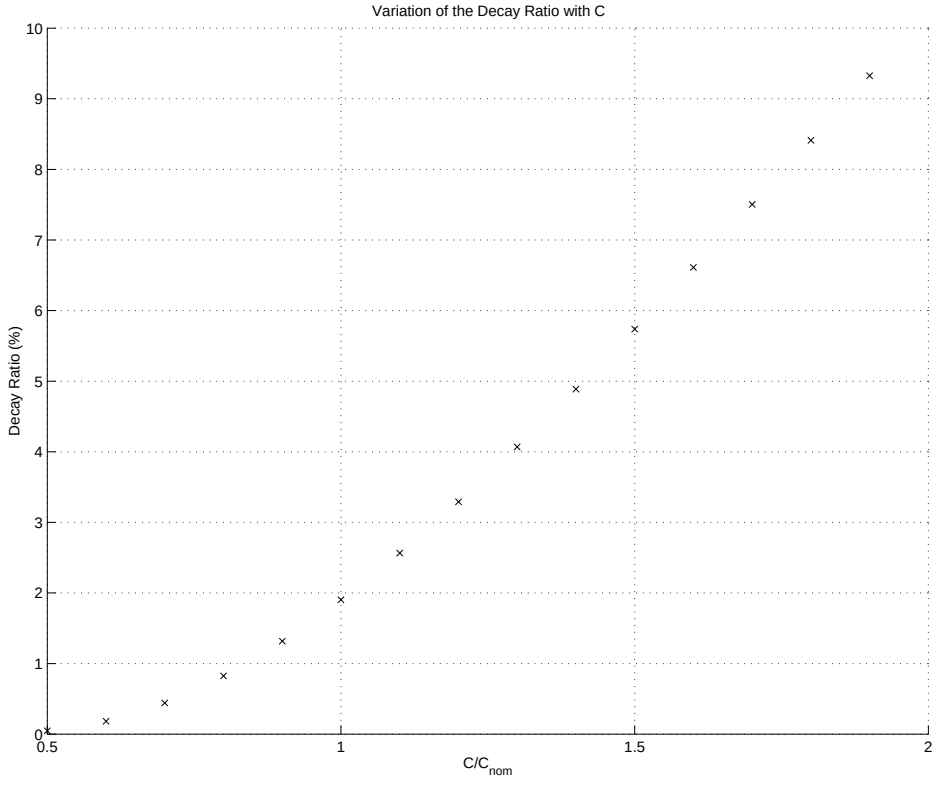

Fig. 21 Analysis of the Effect of *C* on Stability

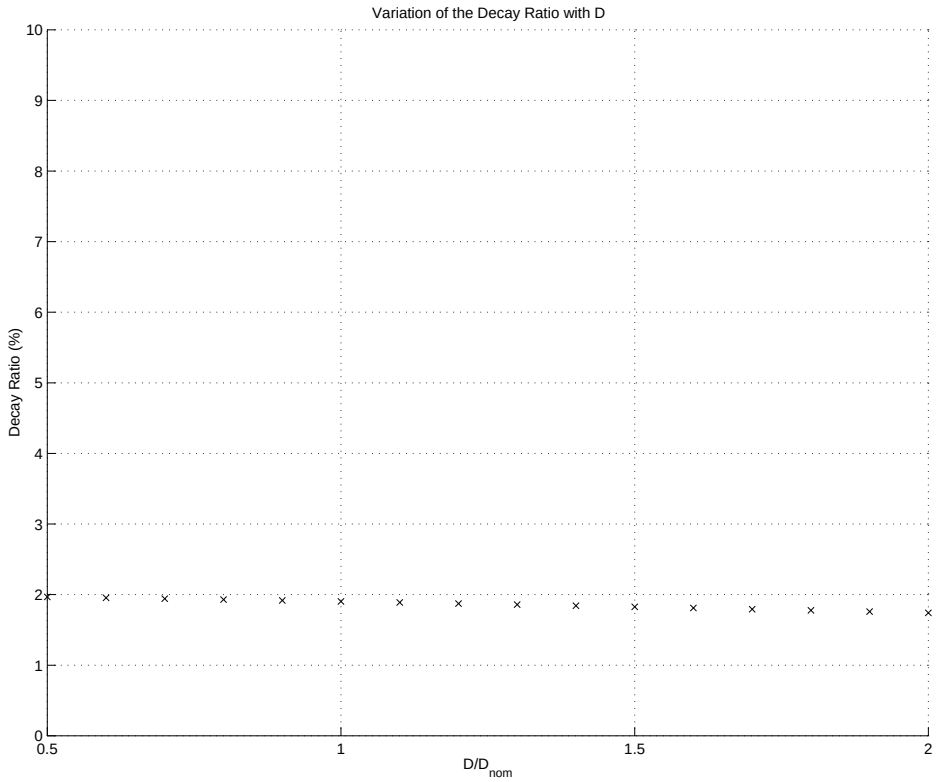

Fig. 22 Analysis of the Effect of *D* on Stability

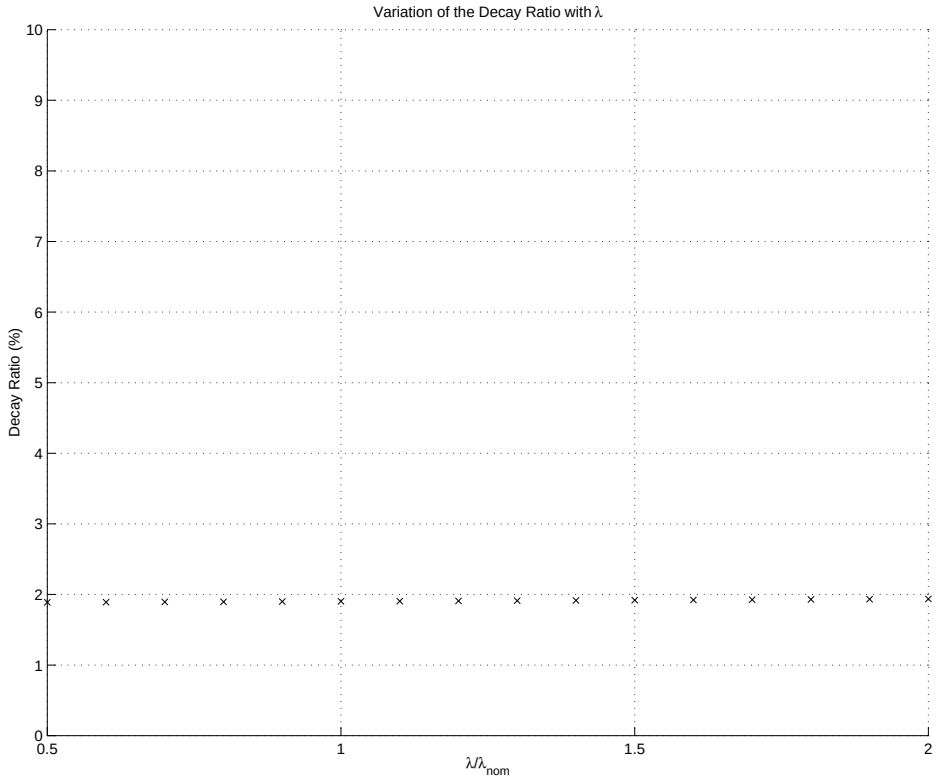

Fig. 23 Analysis of the Effect of λ on Stability

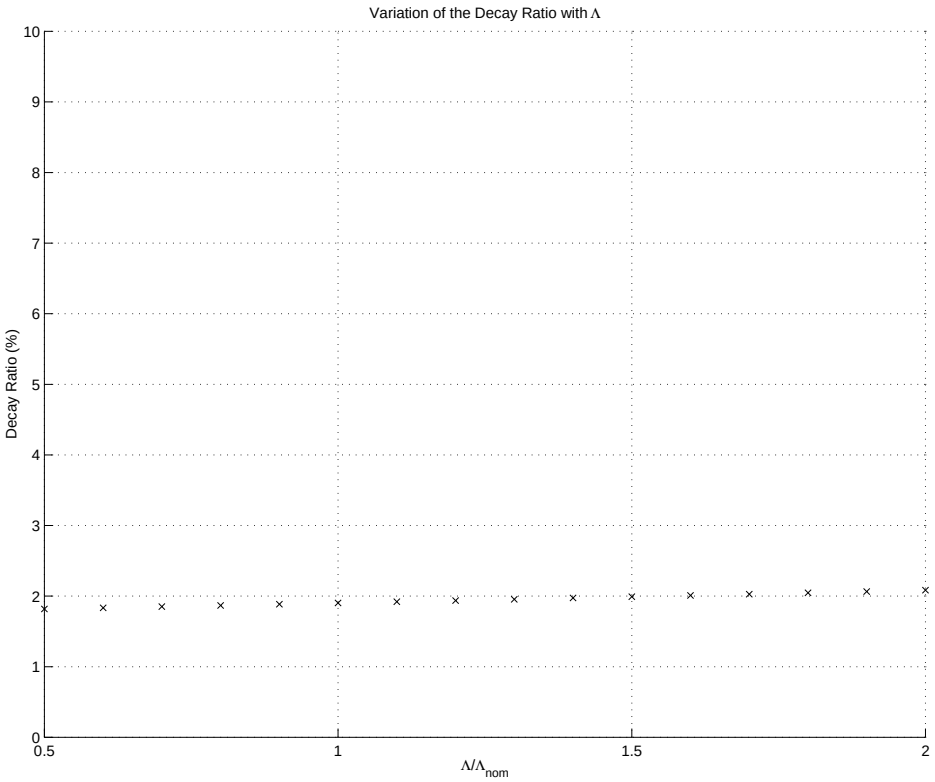

Fig. 24 Analysis of the Effect of Λ on Stability

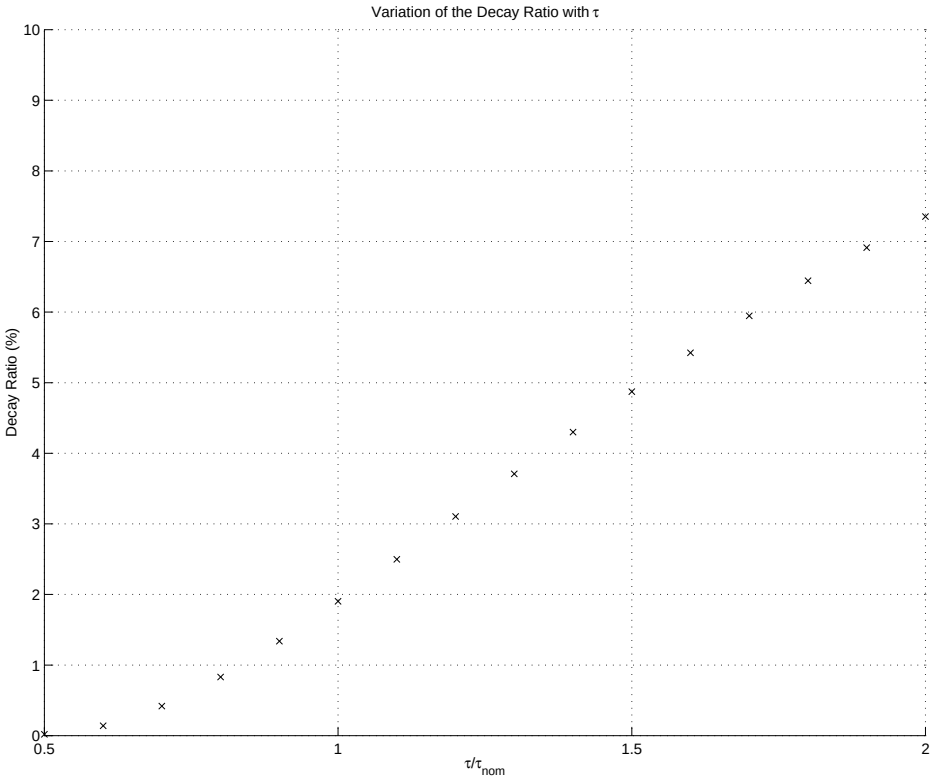

Fig. 25 Analysis of the Effect of τ on Stability

From this preliminary study, it is clear that the most important parameters for the core stability are β_{eff}, a_1, C, and τ. It remains now to study the variation of these parameters with the different core configurations.

τ is representative of the channel thermal-hydraulic properties, so that it is independent of the fuel type that is used (either UOX or MOX fuel). This is why τ is almost constant between the different core configurations.

The DR is also insensitive to the a_2 coefficient. This coefficient is nevertheless slightly larger for the MOX cores since it can be approximated by:

$$a_2 \approx \frac{2h}{\rho_f c_f R_f} \tag{37}$$

and since ρ_f is smaller for MOX fuel (lower fuel density). h, ρ_f, c_f, and R_f are the heat exchange coefficient, the fuel density, the fuel mass heat capacity, and the fuel pellet radius. Furthermore, during the cycle, the fuel temperature increases. As the heat capacity c_f is temperature dependent and decreases with it, a_2 becomes larger at EOC.

Then, the stability of the MOX cores is lower since:

- β_{eff} is lower for the MOX cores (see the reactivity coefficients analysis in § 4.1). β_{eff} decreases also during the cycle (except for the full MOX core).
- a_1 is slightly larger for the MOX cores since it can be approximated by:

$$a_1 \approx \frac{\bar{q}_0}{\rho_f c_f} \tag{38}$$

  and since ρ_f is smaller for MOX fuels (lower fuel density). Furthermore, during the cycle, the fuel temperature increases. As the heat capacity c_f is temperature dependent and decreases with it, a_1 becomes larger at EOC.
- C is larger for the MOX cores (more negative) since the steady-state analysis of the different cores has shown that the void coefficient is slightly larger for MOX bundles (more negative). C decreases also during the cycle (becomes more negative).

Consequently, the stability of the MOX cores decreases since β_{eff} is lower, and a_1 and C are larger. Furthermore, the DR increases during the cycle because β_{eff} decreases (except for the full MOX core), and a_1 and C are bigger.

If one studies the dependence of the DR with the Pu isotopic vector (see Fig. 26), one notices that the DR decreases significantly at BOC if one reduces the Pu-240 content or/and one increases the Pu-239 content. This is due to the fact that in these cases, the void coefficient and consequently the C parameter are less negative (see the steady-state analysis), thus improving the stability. This stability improvement disappears during the cycle because of the fuel depletion.

The following Table VIII summarizes the results of the stability calculations for the mixed UOX/MOX core (base Pu isotopic vector) and the full MOX core. Only the comparison with the full UOX core is presented since this simple model does not allow an absolute determination of

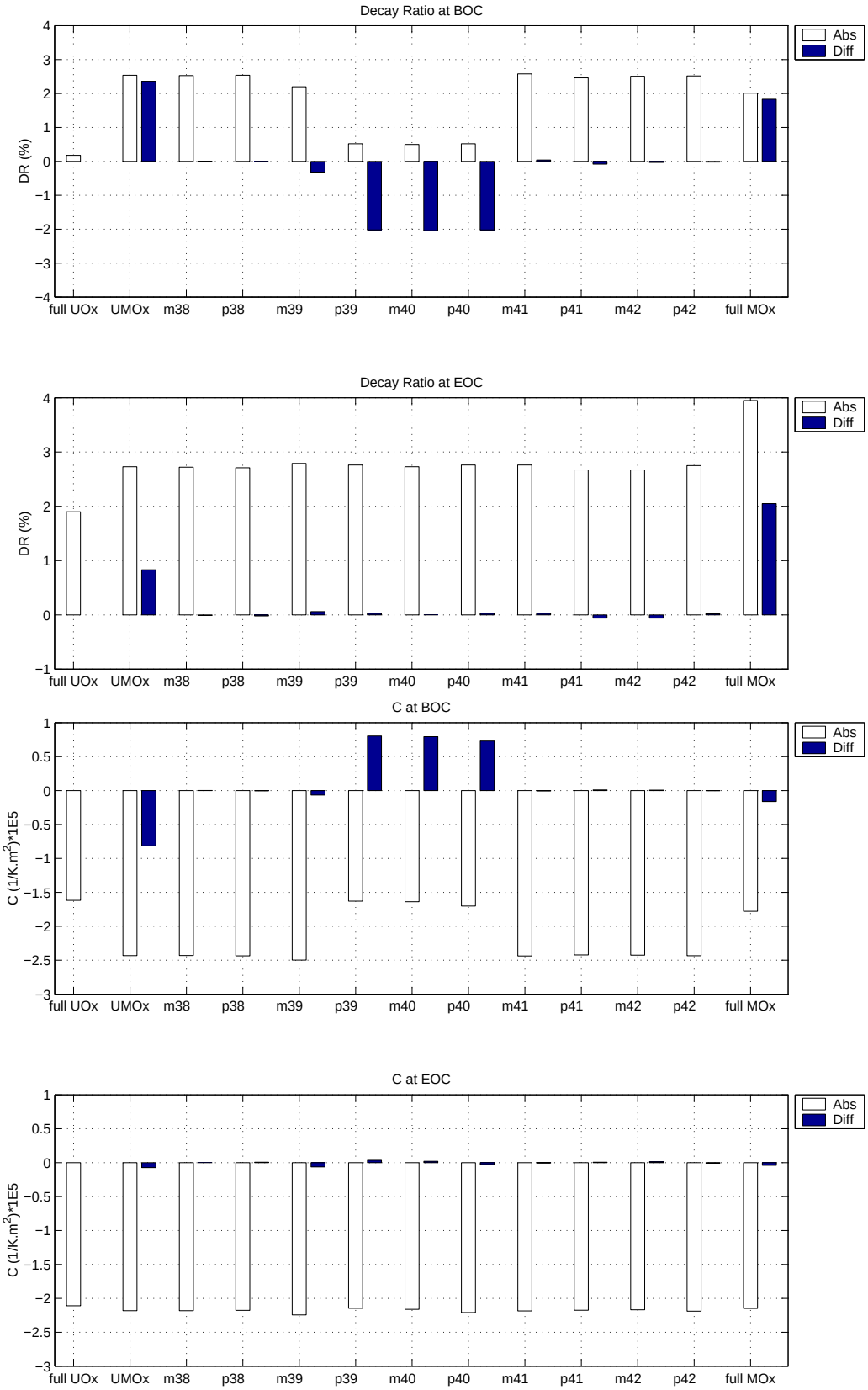

Fig. 26 Analysis of the Stability

the Decay Ratio, i.e. only a qualitative analysis is possible. For a quantitative analysis, one needs a transient code like SIMULATE-3K, or RAMONA.

Table VIII: Stability of the Mixed and Full MOX Cores (at Full Power and Full Core Flow)

	Ratio between the UOX/MOX core DR and the full UOX core DR (absolute DRs)	Ratio between the full MOX core DR and the full UOX core DR (absolute DRs)
BOC	14,11 (2,54 %/0,18 %)	11,17 (2,01 %/0,18 %)
EOC	1,44 (2,73 %/1,90 %)	2,08 (3,95 %/1,90 %)

One notices also that the mixed and full MOX cores are much less stable at BOC than at EOC in comparison with the full UOX core. This is mostly due to the fuel depletion and the production of Pu isotopes by the fresh UOX bundles in the full UOX cores, so that the differences in the core characteristics die out with burnup. Although the MOX cores (mixed UOX/MOX and full MOX cores) are more than ten times less stable at BOC, full power, and full core flow than the full UOX core, it is not possible to conclude anything regarding the stability of each core separately since the absolute DRs are too low to be realistic. It is not granted either that the same ratio can be applied to any part of the power-flow map. This means that the over-simplified March-Leuba model cannot describe properly the stability of one core without any reference to another one, i.e. we cannot say if the DRs are acceptable or not, and if the ratio between the UOX/MOX core DR and the full UOX core DR at full power and full core flow can be extrapolated to other points in the power-flow map (where the stability of the full UOX core is known to be very low).

CONCLUSIONS

The main goal of this study was to determine the ability of BWRs to be loaded with MOx fuels. In order to be able to compare the core characteristics, it was necessary to develop three equilibrium core models: a full UOX core, a mixed UOX/MOX core (approximately 2/3 of UOX bundles and 1/3 of MOX bundles), and a full MOX core. For the two latest ones, a UOX fuel and a MOX fuel have been developed, whereas a typical UOX bundle (defined as a reference case) was used in the full UOX core. All the bundles are of the General Electric BWR 8x8 type. The UOX and the MOX bundles for the mixed and full MOX cores were optimized so that the power distribution is as flat as possible through the depletion, and the cycle length is kept equal to its expected value.

One then noticed that it seems to be possible to load MOX bundles in BWRs (either in a mixed UOX/MOX pattern, or a full MOX pattern), since most of the core characteristics are comparable with the ones of a full UOX core. Nevertheless, two main problems arise:

- the shutdown margin at BOC is lower than 1 %, the value requested by the safety authorities;
- the cores with MOX fuel are less stable.

One way of solving these two problems could have been to modify the Pu isotopic vector: a variation of the Pu-239 and/or the Pu-240 content affects very much both the shutdown margin (SDM) and the Decay Ratio (DR). Unfortunately, these variations are not compatible: if one increases the Pu-239 content for instance, both the SDM and the DR decrease, whereas the opposite behaviour occurs with Pu-240. Consequently, one needs to modify both the Pu quality for the stability and also the control rod efficiency for the SDM, i.e. a new control rod design is necessary. This may be a major obstacle to the loading of MOX fuel, unless the SDM safety limit is lowered.

On the other hand, it is not granted either that the stability of the MOX cores is unacceptable since only a qualitative analysis of the stability has been carried out. This means that an absolute determination of the Decay Ratio for each core is highly recommended. One needs also to scan the whole power-flow map in order to find the high DR regions, in which instability may occur.

Finally, all the calculations in this project and all the analyses have been performed for unrodded cores, i.e. all the rods were out of the cores during the whole cycle. A BWR is never operated this way since the differential worth of a control rod could be negative at the beginning of the insertion. Thus, it could be interesting to look at the modifications of the core properties if the cores are not depleted all rods out, but if most of the reactivity excess is counterbalanced by the rods (a core flow adjustment is also required for an exact compensation). This option has not be chosen for the present study as the control rod pattern could be different for each core type, so that comparing the core properties might become difficult.

ACKNOWLEDGEMENTS

This study was supported by CEA Cadarache, France (DRN/DER/SPRC/LEPh). The author is exceedingly grateful to Drs. Robert Jacqmin and Alain Santamarina. Thanks are also due to all the members of the Department of Reactor Physics in Chalmers, in particular Pr. Imre Pázsit and Dr. Joakim Karlsson, for their help about the stability analysis and their guidance. The Department wishes finally to express his gratitude to Vattenfall for giving financial support to use the Studsvik Scandpower codes.

REFERENCES

1. M. Edenius, K. Ekberg, B. h. Forssén, *CASMO-4 - A Fuel Assembly Burnup Program - User's Manual*, Studsvik Report, Studsvik of America (1993).

2. J. A. Umbarger, *TABLES-3 - Library Preparation Code for SIMULATE-3 - User's Manual*, Studsvik Report, Studsvik of America (1992).

3. J. A. Umbarger, A. S. DiGiovine, *SIMULATE-3 - Advanced Three-Dimensional Two-*

Group Reactor Analysis Code - User's Manual, Studsvik Report, Studsvik of America (1992).

4. Lorne J. Covington, *Generic CMS BWR Equilibrium Model - Revision 1*, Studsvik (1996).

5. H. W. Jr. Graves, *Nuclear Fuel Management*, John Wiley & Sons, United States of America (1979).

6. J. Bussac, P. Reuss, *Traité de Neutronique - Physique et Calcul des Réacteurs Nucléaires avec Application aux Réacteurs à Eau Pressurisée et aux Réacteurs à Neutrons Rapides*, Collection Enseignement des Sciences, Hermann, Paris, France (1985).

7. J. March-Leuba, "A Reduced Order Model of BWR Linear Dynamics", *Nuclear Technology*, **75**, pp. 15-22 (1986).

8. D. Hening, "A Study on Boiling Water Reactor Stability Behaviour", *Nuclear Technology*, **126**, pp. 10-31 (1999).

9. J. K. -H. Karlsson, *Development and Application of Reactor Noise Diagnostics*, PhD thesis, Chalmers University of Technology, Göteborg, Sweden (1999).

10. *State of the Art Report on Boiling Water Reactor Stability*, Committee on the Safety of Nuclear Installations, OECD Nuclear Energy Agency (1997).